Title	Rotational moulding of PEEK polymer liners with carbon fibre/PEEK over tape-placement for space cryogenic fuel tanks
Author(s)	Murray, Brendan R.; Doyle, Adrian; Feerick, P. J.; Semprimoschnig, Christopher O.A.; Leen, Sean B.; Ó Brádaigh, Conchúr M.
Publication Date	2017-07-15
Publication Information	Murray, Brendan R., Doyle, Adrian, Feerick, P. J., Semprimoschnig, Christopher O. A., Leen, Sean B., & Ó Brádaigh, Conchúr M. (2017). Rotational moulding of PEEK polymer liners with carbon fibre/PEEK over tape-placement for space cryogenic fuel tanks. Materials & Design, 132, 567-581. doi: https://doi.org/10.1016/j.matdes.2017.07.026
Publisher	Elsevier
Link to publisher's version	https://doi.org/10.1016/j.matdes.2017.07.026
Item record	http://hdl.handle.net/10379/15604
DOI	http://dx.doi.org/10.1016/j.matdes.2017.07.026

ROTATIONAL MOULDING OF PEEK POLYMER LINERS WITH CARBON FIBRE/PEEK OVER TAPE-PLACEMENT FOR SPACE CRYOGENIC FUEL TANKS

Brendan R. Murray[1], Adrian Doyle[2], P.J. Feerick[2], Christopher O. A. Semprimoschnig[3], Sean B. Leen[1], Conchúr M. Ó Brádaigh[4]

[1]Mechanical Engineering, National University of Ireland Galway, Co. Galway, IRELAND

[2]ÉireComposites Teo, An Choill Rua, Indreabhán, Co. Galway, Ireland, IRELAND

[3]ESA-ESTEC, Materials Space Evaluation and Radiation Effects Section, THE NETHERLANDS

[4]Insitute for Materials and Processes, School of Engineering, The University of Edinburgh, Scotland, UK

ABSTRACT

PEEK polymers are investigated as replacement materials for metallic liners in composite overwrapped pressure vessels (COPVs) for fuel tank applications in space. A novel, integrally heated, rotational moulding tool has been developed to produce PEEK polymer liners, samples of which have then been overwrapped using CF/PEEK in a laser assisted tape-placement (LATP) process to produce demonstrator samples of a polymer lined COPV. Helium permeability testing has shown that the designs are capable of resisting leakage to acceptable levels for fuel storage, while X-ray CT scanning and cryogenic cycling have shown that the current design is capable of resisting crack growth over multiple cycles. Nano-indentation testing has shown that the LATP process has created a region of reduced modulus in the PEEK polymer at the surface of the liner where the CF/PEEK has been tape-laid. This laser-affected zone of reduced polymer modulus in the composite interface region has enabled an enhanced resistance to crack growth formations from thermal residual stresses in comparison to hot plate moulded test samples.

KEYWORDS: Polymers, Composites, Liners, COPVs, Cryogenic Fuel Tanks, PEEK

SYMBOLS:

List of Symbols	
D	Diffusion Coefficient (m^2/s)
E_{IT}	Elastic Modulus (GPa)
J	Leak Rate (scc/m^2s)
P	Permeability Coefficient (scc/m.s.bar)
S	Solubility Coefficient (scc/m^3bar)
x_c	Crystallinity (%)

INTRODUCTION

Composite overwrapped pressure vessels (COPVs) have become a critical component in satellite and space applications since their initial introduction in the early 1970s [1, 2]. Their ability to store highly permeating fuels at high pressures and under cryogenic conditions has solidified their usage in propulsion systems, breathing systems, and manoeuvring systems aboard rockets, satellites, and spacecraft [3-5]. Their light weight configuration, dimensional flexibility, and inherent cost savings has seen them readily incorporated into numerous missions [5-7] while also having significant cross over into other industry sectors such as fire fighter breathing systems and fuel tanks for aircraft and automobiles [8-10].

COPVs consist of two distinct layers: the inner low-permeability liner and the outer high strength fibre overwrap. The thin inner liner acts as a barrier to permeation and limits leakage of the fuel while the outer fibre overwrap contains the stresses generated by the containment of the fuel within. Titanium and aluminium have been the preferred liner materials for space applications [11-13], with Kevlar and carbon fibre epoxies being employed in the overwrapping of the liner [14]. While COPVs have proved exceptional at storing fuels, their main drawbacks are the associated cost of the metallic liner material and the subsequent liner manufacturing costs [15], with recent research focused on creating new and innovative COPV designs [16-23].

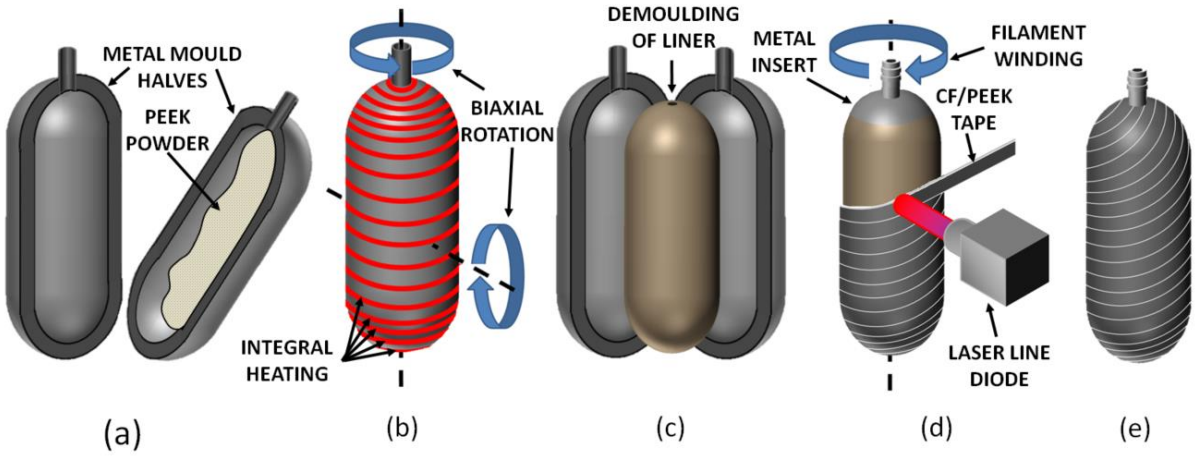

Figure 1. Overview of the complete production process including (a) mould charging with powder, (b) rotational moulding of the liner, (c) demoulding of the liner, (d) over-tape placement using the LATP process, creating (e) a finished COPV.

To this end, polymers have been identified as a viable replacement material for metallic liners in future COPV designs due to their light weight characteristics, low permeability properties, and reduced material costs. A number of studies have already investigated the viability of polymers as low permeability materials [16-24] but little focus has been placed on moulding methods for polymer liner production. While different processes have been used, such as blow injection moulding and thermal welding techniques [19, 20], these methods are capital intensive and have resulted in transferring the cost of production to the tooling, and thus have not significantly reduced the cost of the COPV as a whole. To this end, a modified rotational moulding tool has been constructed as an alternative manufacturing method for low permeability liner production. The commercial advantage of rotational moulding lies in the low cost of the mould tooling, as it is a zero-pressure process [25]. This is particularly suitable for moulding of space fuel tank liners, where the number of components to be moulded may only total in the dozens. These liners, once moulded, can

then be overwrapped with a CF/PEEK tape using a laser assisted tape placement process to form fully functional COPVs using the production process outlined in Fig. 1.

METHODOLOGY AND EXPERIMENTS

MATERIALS AND METHODS

Materials

The materials utilised throughout this research consisted of a number of different polymer and composite materials. For the initial rotomoulding trials and tooling verification, a polyethylene powder from Borealis, Borecene RM8343 [26], was used to qualify the tooling and demonstrate the effective control of heating parameters in the process due to the inexpensive nature of polyethylene powder grades for rotational moulding. For the PEEK polymer liner used for cryogenic fuel storage in the designed COPV, a 50/50 mixture of PEEK 150P and PEEK 150PF from Victrex [27, 28] was used to mould the final liner material. IM7 CF/PEEK from Suprem [29] was used in the production of all composite materials with unidirectional tape grades (nominal width of 140 mm) used for hand laid autoclave samples and (nominal width of 14 mm) for the LATP process. While the composite materials are the same, except for the tape widths, the properties of the parts formed will be dependent on the manufacturing methods employed in their respective production processes.

Hot Plate Moulding

Hot plate moulding of polymer lined COPV samples was undertaken to allow for a comparison to be made to the rotomoulded and LATP overwrapped specimens, as it is a common and inexpensive method of specimen moulding when simulating rotational moulding operations [23]. Hot plate moulding uses a heated metal surface without an applied pressure to mould laminates free of residual stresses. A polymer powder is placed

on the metal surface of the hot plate and is heated until it melts and coalesces together. The heating is then disengaged and the part cools to form a solid component. A representative heating cycle has been included in Fig. 2 to show the similarity in temperature cycles between the hot plate moulded parts and the rotationally moulded parts to be shown later. For the production of demonstrator components, a preformed 8 layer [45°/135°/0°$_4$/135°/45°] autoclaved CF/PEEK Suprem IM7 laminate was placed on the hot plate surface and a layer of PEEK powder was placed on top of the sample. The polymer layer was melted on the composite laminate, through the application of heat (up to 400°C), and then allowed to cool to room temperature to form a demonstrator polymer lined COPV component for testing. These samples were X-ray CT scanned and cryogenically cycled, using the methods explained hereafter, and offer an insight into the differences in properties achieved with the rotomoulding and LATP processes for the current polymer lined COPV design.

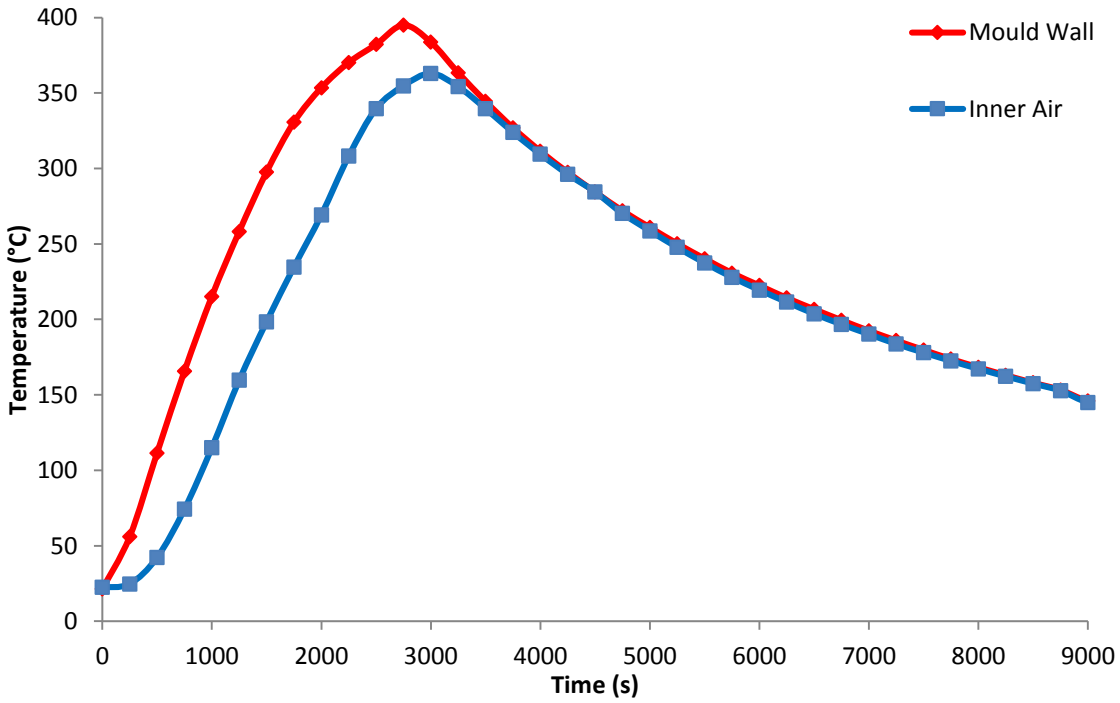

Figure 2. Representative heating cycle for the hot plate moulded PEEK components.

Modified Rotational Mould Tooling

The tooling developed as part of this research is a modified rotational mould tool incorporating an integrally heated electrical system which is placed directly on the tool. The modified tooling removes the need for a large heating oven, which is typical of traditional rotomoulding processes, and increases control of temperature distributions in the mould tool via segregated heating. This enhanced thermal control within the tool increases the dimensional accuracy of parts and improves wall thickness consistencies. The tooling constructed for the current research was fabricated from a number of different materials and systems and can be separated into two main components: the metal mould tool and the heating system. Mild steel plate was the primary mould wall material, with a thickness of 2 mm used throughout the tool. The flange region consisted of a 5 mm thick mild steel plate, with the increased thickness needed to support the mounting of all connections for the rotating rig.

The heating system consisted of three main components; a ceramic resin, a structural glass fibre layer, and the electrical heating lines. The resin consisted of a calcined alumina and calcium aluminate mixture, with the addition of a potassium silicate solution and water in an 80:20 powder to liquid ratio. The heating system used was a HTSAmptek heating tape [30] with an approximate width of 25 mm, a maximum operating temperature of 700°C, and a resistance of approximately 65 Ω (equating to an average length of 200 cm). The glass fibre layer consisted of a +45°/-45° woven fabric which was cut to fit the tooling shape.

The external surface of the metal mould tool was covered in a release film, prior to the heating system application, to mitigate the chances of bonding between the tool and the heating system. This allowed the heating system to expand in an unconstrained manner and

alleviated the risk of cracking in the hardened ceramic layer during heating operations. Once the release film was in place, the heating system was applied in a layered configuration, as outlined in Fig. 3, with the heating lines being sandwiched between two layers of ceramic resin and two layers of fibre glass above and below the heating wires. The heating lines were applied directly beside each other in a linear pattern with no gaps between adjacent lines to ensure consistent temperature distributions across the tools inner mould surface.

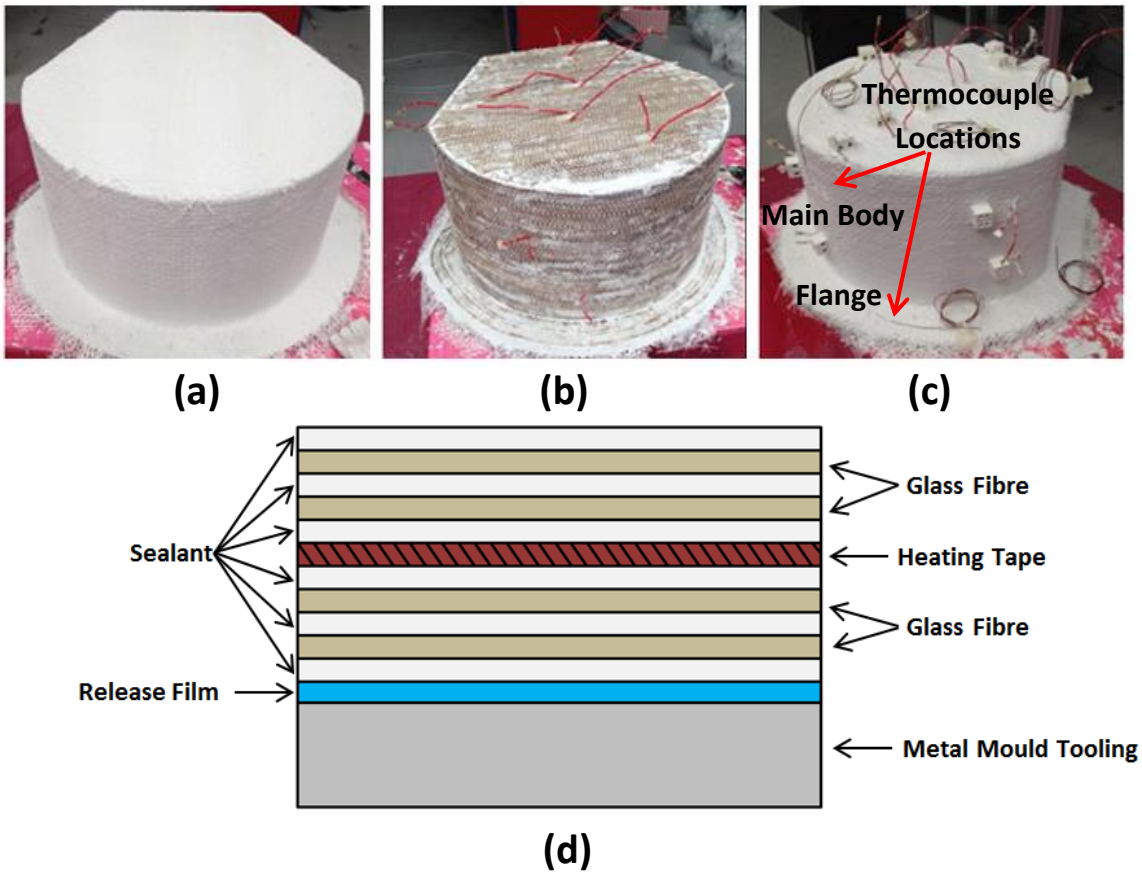

Figure 3. Images showing (a) the initial glass fibre and ceramic resin application, (b) the heating tape application, (c) the finished layered application, and (d) a schematic overview of the layering configuration.

The flange heating region was also segregated from the main body of the tool to allow for enhanced control of the parting line thickness, as the flange behaves in a similar manner to

a cooling fin during heating operations, and as such is the area of greatest heat loss. The temperature control in the flange region is therefore independent to that of the main body of the tool. K type thermocouples were embedded in the heating system at specific locations in the flange and main body as outlined in Fig. 3 (c). The entire rotomoulding system is pictured in Fig. 4 and shows the tooling mounted to the rotating rig which has an internal area of 2.5 m^2 and so allows for the moulding of considerably larger parts.

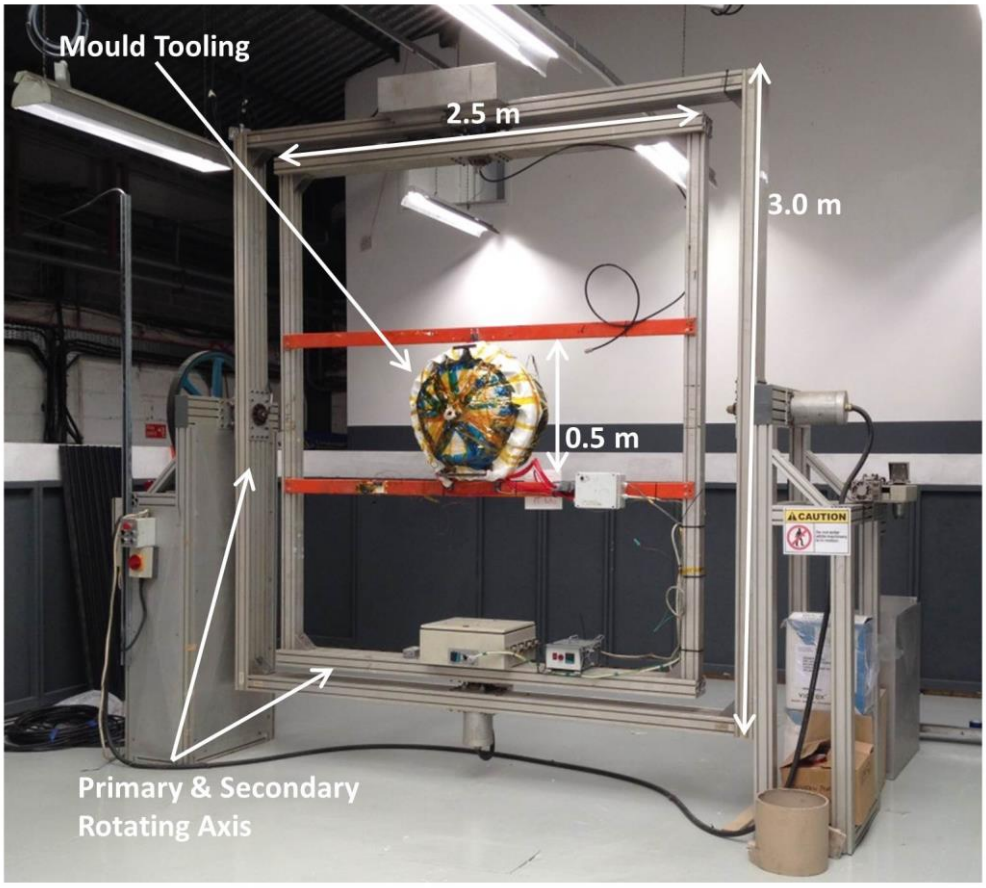

Figure 4. Overview of the rotomoulding configuration including the rotating platform and integrally heated tooling.

The mould tooling is powered via slip ring connections in the joints at the main rotating axes, which transfer power through the rotating arms. The integrally-heated tooling does not significantly affect the temperature of the surrounding area within the turning radius of

the rotomoulding machine and so thermal analysis and control systems can be located directly outside the tool without the risk of thermal degradation. A Testo 881-2 thermal imaging camera, in conjunction with thermocouples imbedded within the heating system, was used to map the temperature distribution across the tooling, with trial runs of polyethylene powders being used to demonstrate the effects of varying processing conditions on part formation. Two different heating cycles, incorporating different flange heating rates, have been used to demonstrate the ability of the tooling to control wall thickness distributions through manipulation of the flange heating parameters.

Laser Assisted Tape-Placement

LATP is an innovative manufacturing method that utilises a robotic arm and an infrared laser to melt and consolidate a thermoplastic composite tape onto a defined surface. It benefits from in-situ consolidation of the composite tape as it is applied, removing the need for post-autoclave processing and decreasing the cost of part formation. The laser moves ahead of the tape and heats both the incoming tape and the substrate surface to the required processing temperature. The tape is then immediately pressed into the substrate through the use of a pressurised roller which consolidates the tape to the substrate and induces proper bonding between individual layers [31-33]. The tape-placement occurs at around 8 to 12 m/min [32, 33] and so the process is equivalent to comparative automated tape-placement methods such as hot gas heating and infrared lamp heating (3 to 9 m/min) [34-36]. While some previous research in LATP forming methods has been conducted [37, 38], a renewed emphasis on LATP methods has emerged in recent years with a focus on fracture testing of CF/PEEK composites [32, 33], LATP thermal process modelling [31, 39-41], and COPV overwrapping modelling [42] at the forefront. The main barrier to LATP acceptance

has been the lower mechanical performance of the tape-laid structures, when compared to autoclaved structures, with improvements in pre-preg properties and processing parameters needed to achieve similar mechanical properties [32]. Specific differences in void content and crystallinity percentages are highlighted as the main factors governing the differences in LATP and autoclave characteristics, with a drive towards process optimization to achieve a better balance in LATP characteristics [32, 33].

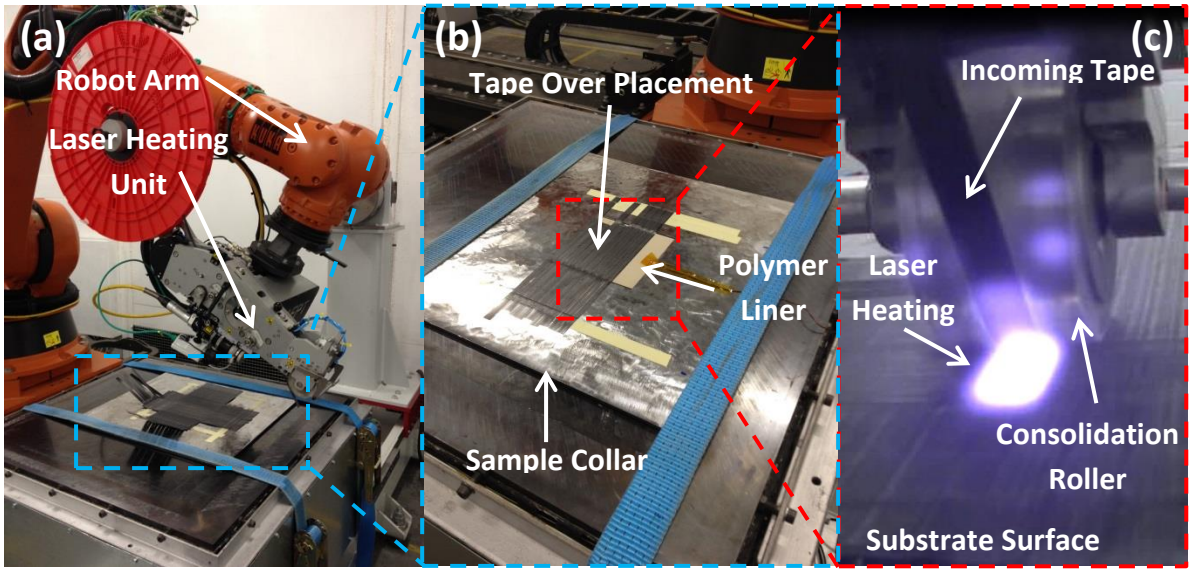

Figure 5. (a) The LATP machine with (b) the metal collar used to facilitate the over tape-placement of samples and (c) an overview of the laser heating system during operation.

The LATP unit used here for the over tape-placement of polymer liner components is displayed in Fig. 5 (a) and consisted of a robotic arm (KUKA KR 180 R2900) with six axes of motion. For tape-placement on polymer liner samples, a mild steel plate was used to accommodate the run in and run off of the LATP process, Fig. 5 (b), as it takes a nominal length of 150 mm of tape for the processing conditions to reach equilibrium conditions, and the metal plate allows for a continuous sample height to be used throughout the LATP process. The tape heating is assisted through the use of a 3000 W laser-line diode module

(LDM) system (supplied by Advanced Fibre Placement Technology (AFTP) GmbH), Fig. 5 (c). The over tape-placement consisted of applying an 8 layer $[0°/90°/0°/90°]_S$ Suprem IM7 CF/PEEK tape onto the PEEK liner substrate and constituted a demonstrator component for further testing of the current polymer lined COPV design. The lay down speed used was 12 m/min and the material temperature at the tape application point was 380°C. A silicone roller was used to consolidate the tape to the polymer liner surface with an applied pressure of 4.5 bar.

Permeability Testing

The permeability testing conducted here followed the standard test method as outlined in ASTM D1434 [43]. Each sample was clamped between two aluminium chambers and a vacuum was applied to both sides of the sample to remove any residual gases. Once the downstream chamber reached a significantly low vacuum, the helium leak rate detector, a Leybold L200, was engaged. Helium test gas with a purity of 99.999% was then pumped into the upstream chamber, at an applied pressure of 1.15 bar, and permeated through the sample over time. “Leakware” software was then used to map the leak rate through the sample and these results were used to calculate the resultant permeability coefficients. Leak rates, *J*, permeability coefficients, *P*, diffusion coefficients, *D*, and solubility coefficients, *S*, have been obtained for each material configuration using the time lag method of analysis as previously outlined [22]. This is a standard method used to define permeability coefficients for materials based on precise measurements of gas leak rates at steady state conditions and constant leak rates [22, 44, 45]. Tests lasted anywhere from 12 to 48 hours depending on the material thickness and the samples intrinsic material properties.

Three samples per material have been tested for leak rates. These results were used to define coefficients for the individual materials in the COPV design. This includes:

- (L1) The rotomoulded PEEK liner material;
- (L2) An individual 8 layer $[0°/90°/0°/90°]_S$ LATP CF/PEEK Suprem IM7 sample;
- (L3) The full polymer lined COPV design consisting of a rotomoulded PEEK liner with an 8 layer $[0°/90°/0°/90°]_S$ CF/PEEK Suprem IM7 LATP over tape-placement;
- (A1) An autoclave formed $[45°/135°/0°_4/135°/45°]$ Suprem IM7 composite laminate;

The latter is used to provide a comparison between the different moulding methods and their effects on each configuration's intrinsic permeation resistance. The individual results for the PEEK liner and LATP over tape-placed materials have also been used to predict the leak rates of the final combined liner design and have been compared to the measured experimental results for the over tape-placed samples.

Differential Scanning Calorimetry

Differential scanning calorimetry (DSC) has been used to assess the crystallinity of polymer and composite components moulded using different processing methods. DSC is a thermal analysis technique that determines the melting temperature and crystallinity percentage of materials by measuring the heat required to increase the temperature of a small sample of the material and comparing the result to that of a 100% pure sample. DSC testing was conducted using a Shimadzu DSC-60 based on the heat-flux method. Five samples of each material were tested with Shimadzu aluminium crimp pans (SH201-52943) following ISO 11357-1 [46], ASTM D3418-12 [47] and a heating rate of 20 °C/min. The value for heat of fusion for a 100% crystalline PEEK material has been taken from published literature (130

J/g) [48] and has been used to assess the crystallinity of all PEEK polymers and composites tested here. The DSC measurement obtained for the PEEK composite materials must be altered to consider the mass fraction of the composite fibres in the sample to provide a true value of crystallinity [49-51]. Higher crystallinity usually equates to lower permeability [52-55], and as such crystallinity is an important factor governing permeability.

Cryogenic Cycling

Thermal cycling trials were performed on the LATP liner-over tape-placed samples to simulate the filling of a COPV fuel tank with a cryogenic fuel. Cryogenic cycling induces a residual stress build-up in the samples due to the differences in coefficients of thermal expansion between the polymer liner and composite, and tests the susceptibility of the design to delamination, fracture, and overall liner integrity over the rapid change in temperature. The thermal cycling process involved immersing samples into liquid nitrogen for two minutes, to simulate the cryogenic cooling process to temperatures below 77 K (-196 °C). Samples were then removed from the liquid nitrogen and heated to ambient temperatures over a further eight minute period constituting a single cryogenic cycle as is consistent with standard methods [56-59]. Samples were cycled up to fifty times and their internal structural integrity was monitored with X-ray CT scanning.

X-ray CT Scanning

Intermittent X-ray CT scanning was performed on the samples between cryogenic cycles to analyse the samples internal structure, at the bond interface between the liner and composite, during repeated cryogenic cycles which allowed for the monitoring of internal crack growth over time. X-ray CT scanning has been used by a number of authors for

analysing polymer and composite materials, specifically in the area of void and microcrack mapping [22, 32, 59-64]. The majority of analyses conducted for COPV applications have centred on epoxy composites with graphite [65, 66] and carbon fibres [57, 67-70], with limited analyses of carbon fibre PEEK composites [59, 71], and even less so for LATP CF/PEEK laminates [42, 72].

The X-ray CT machine used here was a GE V/tome/X m300 with a Microtom gun operating at a voltage of 230 kV and 60 µA, giving a scan power of 13.8 W. The sample was rotated through 360° while over 1000 X-ray images were taken, and these images were used in conjunction with VG Studio Max 2.2 software, to render a 3D model which was then used to analyse internal defects and cracks. Significant clarity of the samples internal structures after cryogenic cycling has been obtained with voxel sizes of less than 10 µm achieved (nominally based on sample size, position, and X-ray settings). Polymer liner samples, which had been over tape-laid with the LATP process, were assessed using X-ray CT scanning before cryogenic cycling, and after 1, 2, 3, 5, 10, and 50 cryogenic cycles respectively. The results of these analyses are compared to hot plate moulded polymer lined COPV samples to demonstrate the differences in thermal residual stress build up on cracking and liner failure.

Nano-indentation Testing

An assessment of the effects of the laser heating process on the PEEK liner was also undertaken using nano-indentation on the sample cross section to determine the change in elastic modulus, E_{IT}, at the PEEK liner material interface. The laser melts the polymer liner surface during processing to form the bond between the CF/PEEK tape and the PEEK liner surface. However, this rapid heating and rapid cooling changes the structure of the polymer

liner at the bond interface. Nano-indentation testing characterises the mechanical properties of a material on a microscopic level using an indenter tip, with a known shape, to indent the sample while measuring the applied force and displacement during loading and unloading of the sample [73-77]. Testing was performed with a nano-indenter (CSM Instruments SA, Switzerland) following ASTM E2546 [73] using a pyramidal Berkovich diamond indenter tip, in conjunction with the Oliver and Pharr method of material property analysis [77]. The Berkovich tip factors used were consistent with standard practices [73-77] while the Poisson's ratio of PEEK had an assumed value of 0.38 [78].

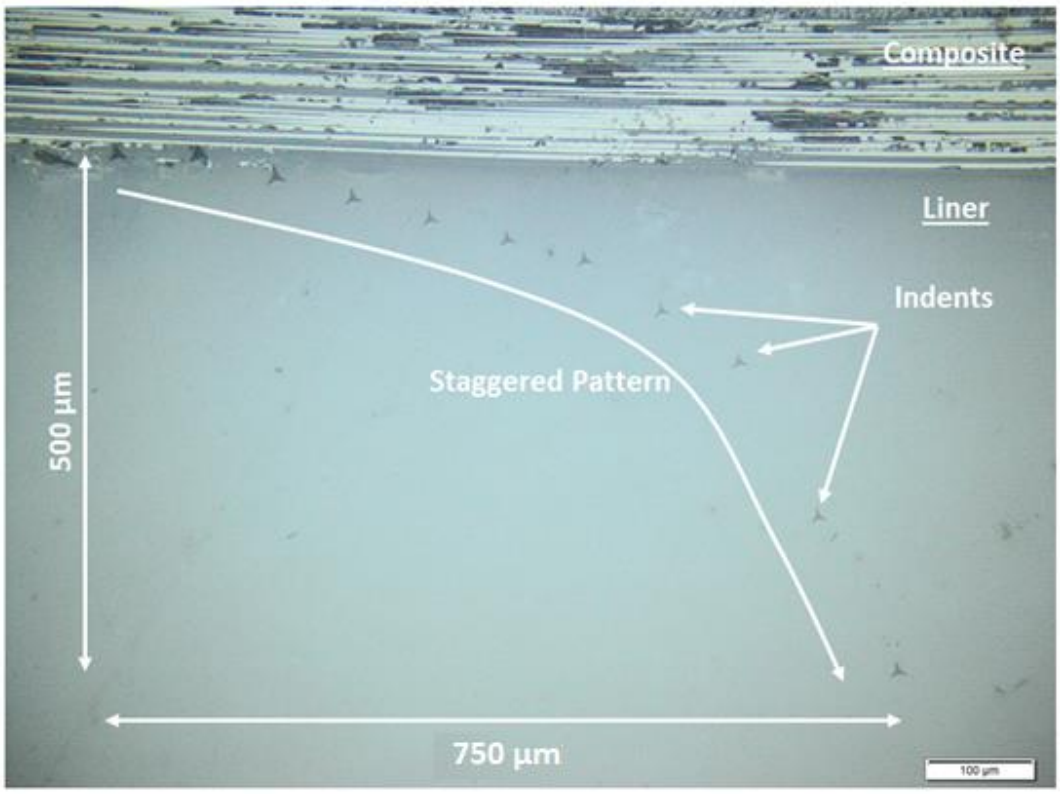

Figure 6. Microscopy image of the indentation analysis carried out on the liner-overwrap samples showing the staggered acquisition pattern.

Small cross sections of PEEK polymer liner samples, that were over tape-placed with 8 layers of CF/PEEK in the LATP process, were removed and mounted in an epoxy resin and polished

with increasingly finer SiC grit papers (from 1200 up to 3200) and then a 0.06 µm alumina suspension. A number of nano-indentation studies have been carried out by other authors on PEEK [79-81] and PEEK composite materials [82-84] with varying test parameters used. For the present study, the nano-indentation parameters included an applied load of 40 mN, a loading and unloading rate of 80 mN/min, and a hold time of 20 s. These parameters have given a nominal Young's modulus of 5 GPa which is consistent with published results. A minimum spacing of 75 µm was maintained between indents to avoid discrepancies due to overlapping fields of elastic deformation [85]. Eleven indents were performed per test in a staggered pattern, as shown in Fig. 6. The first indent in every test was a depth calibration to ensure consistent measurements across all tests. This scheme allowed for the minimum distance between indents to be maintained while incrementally increasing the distance of the indents outward from the bond line between the liner and tape-laid sample.

RESULTS AND DISCUSSION

Tooling Design

Two different temperature cycles were applied to the tooling to highlight the difference in flange heating control optimisation. The first trial run, whose heating trace is outlined in Fig. 7, shows the effects of heating the flange and main body at the same rate for the entire heating cycle. In Fig. 7, the inner air temperature is higher than the corresponding mould tooling temperature which is not directly the case within the tooling. This is due to the inner air temperature being measured directly from the tooling vent while the mould tooling temperature is taken from outside the heating lines where the thermocouple is embedded in the heating system. In this way the mould tooling measurement can lag behind the inner air measurements as it has a layer of materials between it and the mould surface

measurement. In reality the mould wall temperature should always be greater than the inner air temperature. The second trial run, Fig. 8, utilises an optimised flange heating approach, designating the flange as a single zone such that heating at the parting line can be altered to keep the temperature distribution uniform across the wall section of tool which in turn enhances wall thickness consistencies. This is demonstrated by heating the flange region to the melting point of polyethylene, over a 10 to 15 minute period, prior to engaging the heating in the rest of the tool. In this way, the flange region near the parting line will start to melt polymer powder particles at an earlier stage in the process, in comparison to the main body of the tool, and so the wall thickness build up will be increased in this region to compensate for the heat loss experienced at the parting line.

A thermal imaging camera was used to characterise the two heating cycles individually in a separate analysis to examine the temperature distribution inside the tool, Fig. 9 (a), during the heating cycle. Fig. 9 (b) shows the thermal image of the internal tool surface for the first cycle involving the uniform heating rate across the entire mould tooling. Here the temperature near the flange is lower than the surrounding mould tooling from the start of the heating cycle right through to the end with 20 °C temperature differences recorded. In contrast the second heating cycle has the opposite effect. Fig. 9 (c) shows that the area near the flange heats at a faster rate than the rest of the tool and so the flange region nearest to the parting line is now the hottest part of the tool. This will continue throughout the cycle and allows the parting line region to be at a uniform temperature with the rest of tool for the duration of the moulding process to enhance powder pick up consistencies during component formation.

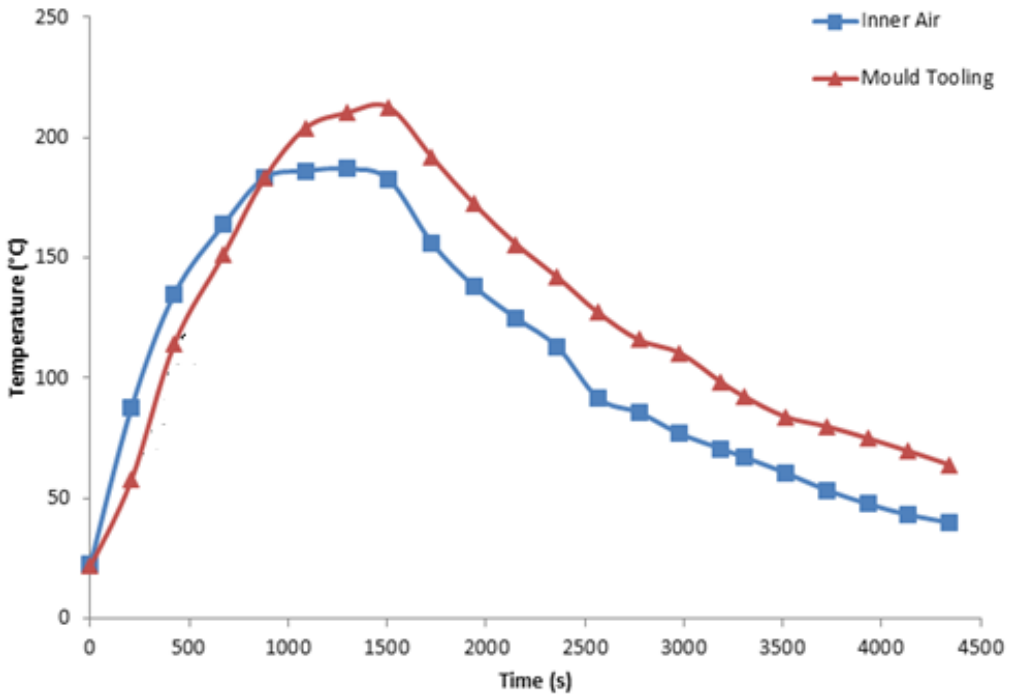

Figure 7. Measured heating trace for the integrally-heated tooling using equal heating across the tooling.

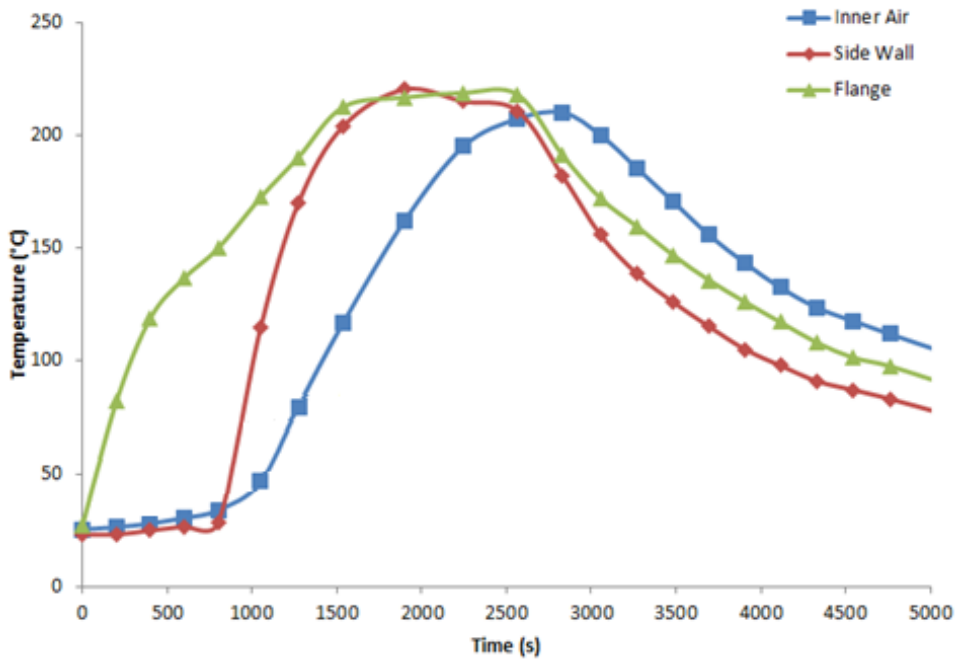

Figure 8. Measured heating trace for the integrally-heated tooling where flange optimisation has been used to promote uniform temperature distributions in the tool.

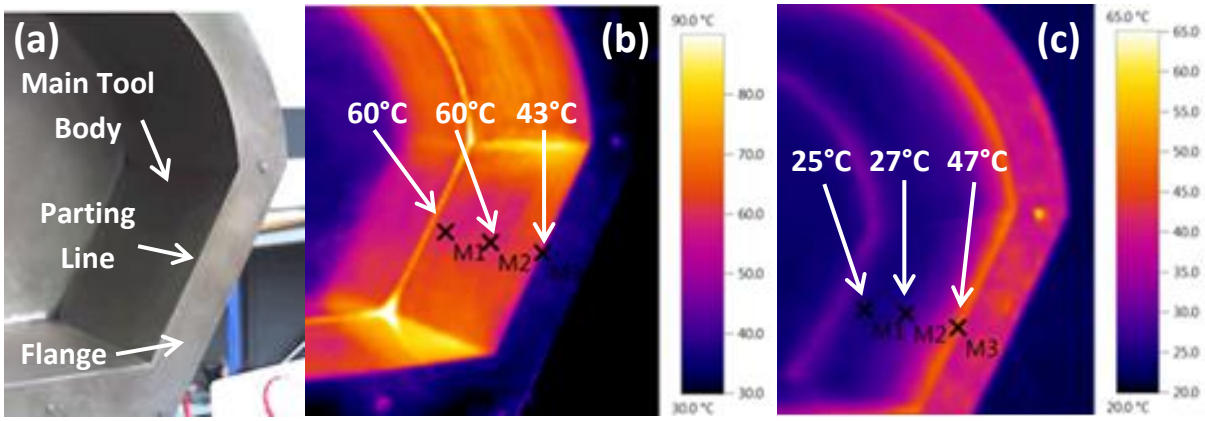

Figure 9. (a) A digital image of the thermal analysis performed with (b) a thermal image of the uniform heating leading to lower parting line temperatures and (c) a thermal image of the optimised flange heating, giving higher flange temperatures to mitigate heat loss in the region and to promote more uniform temperature distributions.

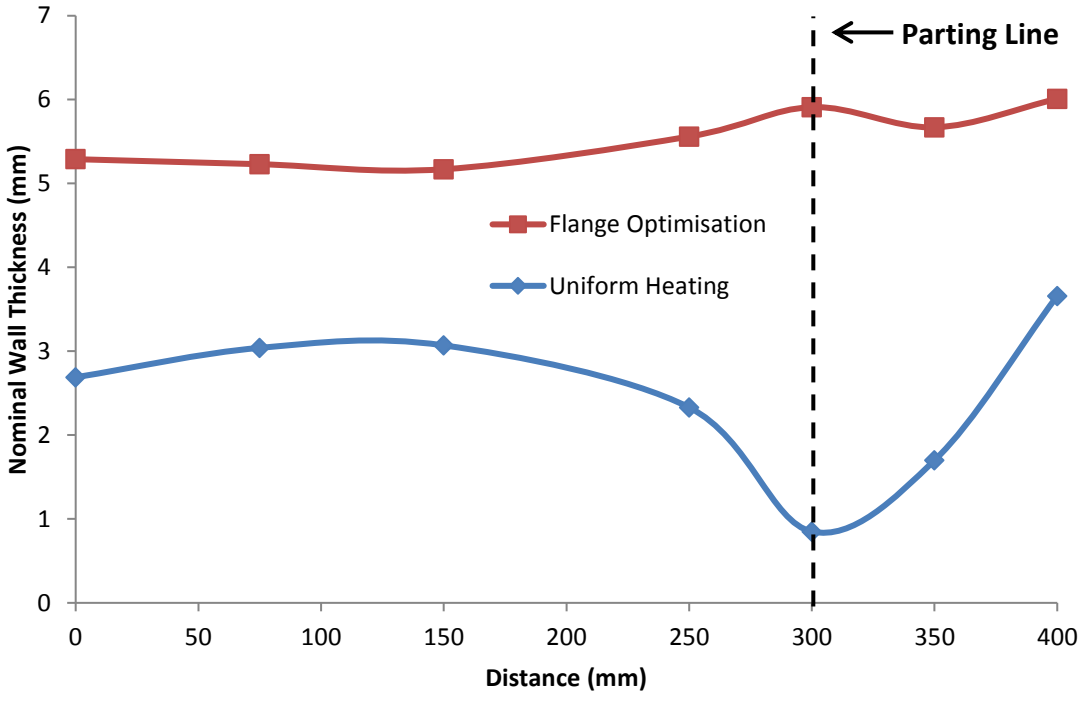

Figure 10. Wall thickness distribution measurements for both the uniform heating cycle and the optimised flange heating cycle, showing the improved wall thickness consistency.

The demonstrator parts produced from these two heating cycles were then analysed for wall thickness consistencies to demonstrate the improvements achieved with flange heating optimisation. Fig. 10 shows the average wall thickness distribution of each demonstrator moulded, with the first cycle using uniform heating showing a sporadic distribution with a significant decrease in thickness at the parting line (300 mm mark on the distance length). The second cycle shows a clear and consistent linear distribution which is superior to the first heating cycle. The flange heating at the parting line is clearly beneficial for part consistency and highlights the enhanced level of control achievable.

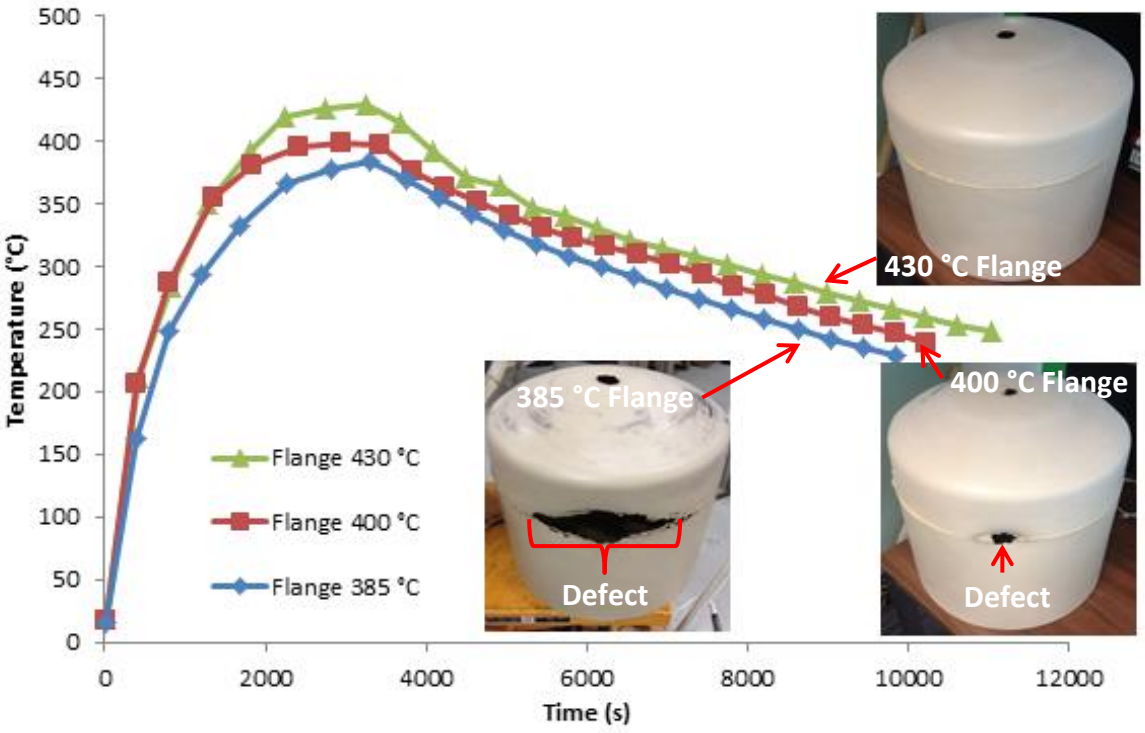

Figure 11. Flange heating profiles for three separately rotomoulded PEEK tanks with the effects on the parting line consolidation highlighted.

This process has also been used to optimise the production of PEEK polymer liners, whereby segregated flange heating was used to increase the consistency of wall thickness distributions of PEEK demonstrator components at the parting line. Fig. 11 shows three

different flange heating cycles used to form three different PEEK liners with the inset images showcasing the parting line inconsistencies of the lower temperature flange heating cycles. The flange temperature was increased for each subsequent cycle until the parting line defects were removed, in an iterative process, and in this way the flange heating was optimised. The use of the higher flange heating has overcome the heat loss effects of the flange region and allowed for the production of a consolidated liner without defects at the parting line as displayed by the photos of finished demonstrators within Fig. 11. The same powder mass was used in all tanks pictured and so the change in flange wall thickness distribution can be solely attributed to the flange optimisation procedure.

Permeability Test Results

Permeability testing was performed on all materials used in the formation of the polymer lined COPV demonstrator. An allowable leak rate of 1 x 10^{-3} scc/s has been set for the 90L COPV designed here, with the COPV having an assumed internal surface area of 1 m^2, and operating at a pressure of 5 bar. This equates to an allowable leak rate of 2.3 x 10^{-4} scc/m^2s for helium testing at 1.15 bar through the use of Fick's law [44, 86] to equate the set conditions at 5 bar to the lower test pressure of 1.15 bar. The results, Table 1, show that the rotomoulded PEEK polymer liner samples (L1) have the highest leak rate and permeability coefficients of all the materials tested. These results are consistent with previously tested hot plate moulded PEEK samples which had permeability coefficients of between 6.5 x 10^{-7} scc/m.s.bar and 7.3 x 10^{-7} scc/m.s.bar for Victrex PEEK materials [22].

Table 1 also shows good correlation between permeability coefficients of the Suprem IM7 CF/PEEK LATP samples (L2) and the Suprem IM7 CF/PEEK autoclave samples (A1), with values of 1.12 × 10^{-7} scc/m.s.bar and 0.87 × 10^{-7} scc/m.s.bar respectively. The difference in

permeability coefficients could potentially be attributed to the differences in crystallinity between the respective samples as higher crystallinity usually equates to lower permeability [52-55], with the autoclaved samples (A1) having a higher crystallinity of 44.47%, in comparison to the LATP samples (L2) which have a lower average crystallinity of 35.00%.

Table 1. Permeability results for polymer and composite materials in the COPV design

I.D.	Specimen	Thickness (mm)	J Leak Rate (10^{-5} scc /m^2s)	*P* (10^{-7} scc./ m.s.bar)	*D* (10^{-11} m^2/s)	*S* (10^3 scc/m^3 bar)	x_c (%)
L1	PEEK	3.13 (±0.87)	46.3 (±10.8)	11.1 (±1.24)	1.56 (±0.37)	7.69 (±1.26)	39.0 (±4.23)
L2	LATP CF/PEEK	1.23 (±0.01)	10.4 (±3.54)	1.12 (±0.37)	14.5 (±17.6)	2.30 (±2.53)	35.0 (±3.17)
L3	Rotomoulded PEEK-LATP	6.20 (5.0/1.2) (±0.08)	9.42 (±5.49)	5.5 (±2.88)	16.1 (±8.41)	3.10 (±0.23)	L1/L2
A1	Autoclave CF/PEEK	1.18 (±0.01)	8.40 (±0.79)	0.87 (±0.09)	2.27 (±0.12)	3.81 (±0.24)	44.47 (±4.16)

Note: All tests were carried out with helium test gas at an applied pressure of 1.15 bar, while the figures in brackets indicate a single standard deviation.

This is to be expected as the autoclave samples go through a much slower cool down process and hence have higher crystallinities than the LATP samples which are rapidly cooled in air after the laser heating and melting process and so have a much lower crystallinity. The connotation L1/L2, for the crystallinity of L3, defines that L3 is formed from the combination of both materials L1 and L2 and so has a crystallinity which is equal to both materials in their constituent locations in the part design. While this is one variable affecting the permeability of both materials, it is more likely that the internal defects and voids

created by the inconsistency of the LATP process are the cause of the higher permeability coefficients of the LATP samples, as will be demonstrated later via X-ray CT scanning.

The main result to highlight from these tests is the low leak rate of the rotomoulded PEEK liner material over tape-placed with the LATP Suprem IM7 CF/PEEK (L3). The permeability coefficient is higher for this dual layer material in comparison to its composite counterparts, but this is a measurement of the effective permeability and as such is taking the permeability of both materials into consideration during its analysis. The leak rate of the rotomoulded-LATP samples (L3) at 9.42 x 10^{-5} scc/m^2s is lower than that of the individual LATP CF/PEEK samples (L2) and slightly higher than that of the autoclaved CF/PEEK samples (L3). The leak rate of the rotomoulded PEEK LATP samples is well below the set allowable leak rate of 2.3 x 10^{-4} scc/m^2s for the COPV designed here and is almost 60% lower than the stated allowable giving a significant factor of safety to the current design configuration.

The permeability of the polymer lined COPV can also be predicted from the individual permeability coefficients of the PEEK polymer liner (L1), P_{Liner}, and the permeability coefficient of the LATP CF/PEEK overwrap (L2), $P_{Overwrap}$, to predict a value for the dual layer configuration which can be compared to the measured value of the rotomoulded LATP configuration (L3) via [87]:

$$P_{effective} = \frac{1}{\frac{V_{Liner}}{P_{Liner}} + \frac{V_{Overwrap}}{P_{Overwrap}}} \quad (1)$$

with the volumes V_{Liner} and $V_{Overwrap}$ based on the constituent materials relative thicknesses, the predicted effective permeability is 4.04 × 10^{-7} scc/m.s.bar. This is on par with the measured value of 5.05 × 10^{-7} scc/m.s.bar given the relative inconsistency of the LATP

CF/PEEK samples, as will be shown via X-ray CT scanning. This gives an equivalent predicted leak rate of 7.51 × 10^{-5} scc/m^2s for the samples tested here which is also close to the measured value of 9.42 × 10^{-5} scc/m^2s and demonstrates that there is still room for improvement.

The samples were then immersed in liquid nitrogen following the cryogenic cycling procedure outlined. After cryogenic cycling, the composite samples were retested for permeability. The results, Table 2, show an increase in leak rate which is indicative of microcracking in the composite laminates. The majority of cracking has occurred after the first cryogenic cycle in the composite samples, as the leak rate has not increased significantly after continued cryogenic cycling up to ten cycles, which is consistent with published research [59, 72]. The rotomoulded PEEK samples tape-laid with the CF/PEEK tape were also cryogenically cycled, showing visible cracking in the through thickness direction of the liner. This compromises the design's effectiveness as a permeation barrier and as such no leak rate results were obtained for the tape-laid PEEK samples due to the cracking which mitigated the effective sealing of the sample.

Table 2. Leak rates for cryogenically cycled composite laminates.

Material	Thickness (mm)	Pressure (bar)	*J*, Leak Rate (10^{-5} scc/m^2s)		
			0 Cycles	1 Cycle	10 Cycles
Autoclave CF/PEEK	1.18 (±0.01)	1.15	8.40 (±0.79)	12.2	12.3 (±0.69)
LATP CF/PEEK	1.23 (±0.01)	1.15	10.4 (±3.54)	16.2	16.5 (±1.84)

Note: The figures in brackets indicate a single standard deviation, while an error in the measurement of results for 1 Cycle meant that only one sample produced usable results, hence its lack of an accompanying standard deviation.

Cryogenic Cycling and X-ray CT Scanning

As has already been noted, PEEK lined CF/PEEK samples have been moulded on a hot plate and tested under cryogenic conditions to allow for comparisons to be drawn between these and the rotomoulded LATP samples. The samples were X-ray CT scanned before and after a single cryogenic cycle, with the results displayed by Fig. 12 (a) and (b) respectively, showing that the hot plate samples undergo significant failure of the liner after a single cryogenic cycle. This is evidenced by the numerous cracks in the X-ray image in Fig. 12 (b) whereby cracks have propagated through the thickness of the PEEK liner material and have resulted in complete failure of the design. This is due to the significant build up in thermal residual stress that the sample undergoes as it is cooled to cryogenic temperatures. Air voids are also present in the liner region, as they are an intrinsic property of rotomoulded components, but they can be removed via the application of an over-pressure during moulding [25] which was not undertaken for these samples due to a lack of facilities.

The build-up of thermal residual stress in the sample can be identified even before cycling has occurred as the X-ray image in Fig. 12 (a) shows a characteristic bend in the sample which is indicative of the greater shrinkage in the polymer liner (which has a coefficient of thermal expansion of 54 μm/m°C [88]), in comparison to the composite material (which has a coefficient of thermal expansion of 0.2 μm/m°C in the fibre direction and 28.8 μm/m°C in the transverse direction [42]), due to the liner's higher coefficient of thermal expansion. This is from the initial cool down of the sample from the stress free temperature of PEEK (which is 315°C [59]) to room temperature and is further increased by the cool down to cryogenic temperatures, resulting in complete failure of the liner, and a return to a flatter sample structure with the release of the built up residual stress via cracking.

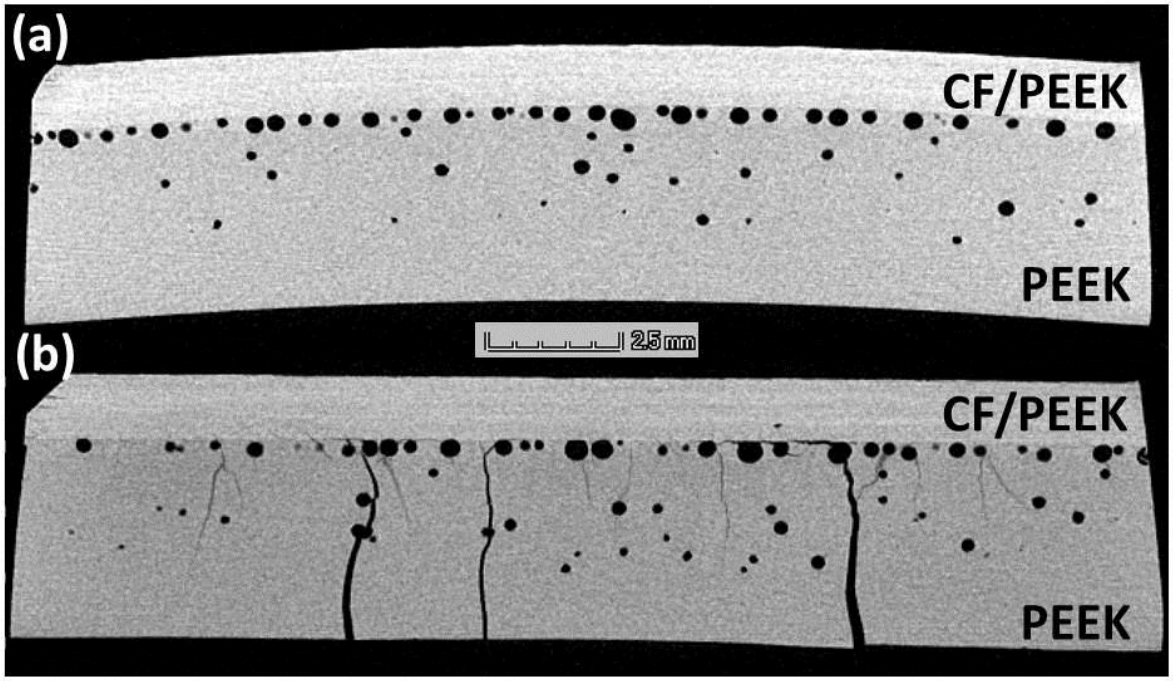

Figure 12. X-ray CT images of the cross section of a PEEK-CF/PEEK hot plate moulded laminate (a) before and (b) after cryogenic cycling with extensive cracking visible.

The extent of cracking in the sample is displayed by a three dimensional reconstruction in Fig. 13 which gives both solid and transparent views of the internal cracking in the sample.The internal structure of the autoclaved CF/PEEK samples (A1) and the LATP CF/PEEK samples (L2) has also been compared using X-ray CT scanning. 20 mm × 20 mm samples were removed from both samples and scanned for internal defect measurements. The analysis consisted of a comparison between the seven individual bond regions between the eight carbon fibre layers in both the autoclave sample, Fig. 14, and the LATP sample, Fig. 15. They are labelled from (1) to (7), (1) being the bottom two layers of the laminate and (7) corresponding to the bonding region between the top two layers of the laminate.

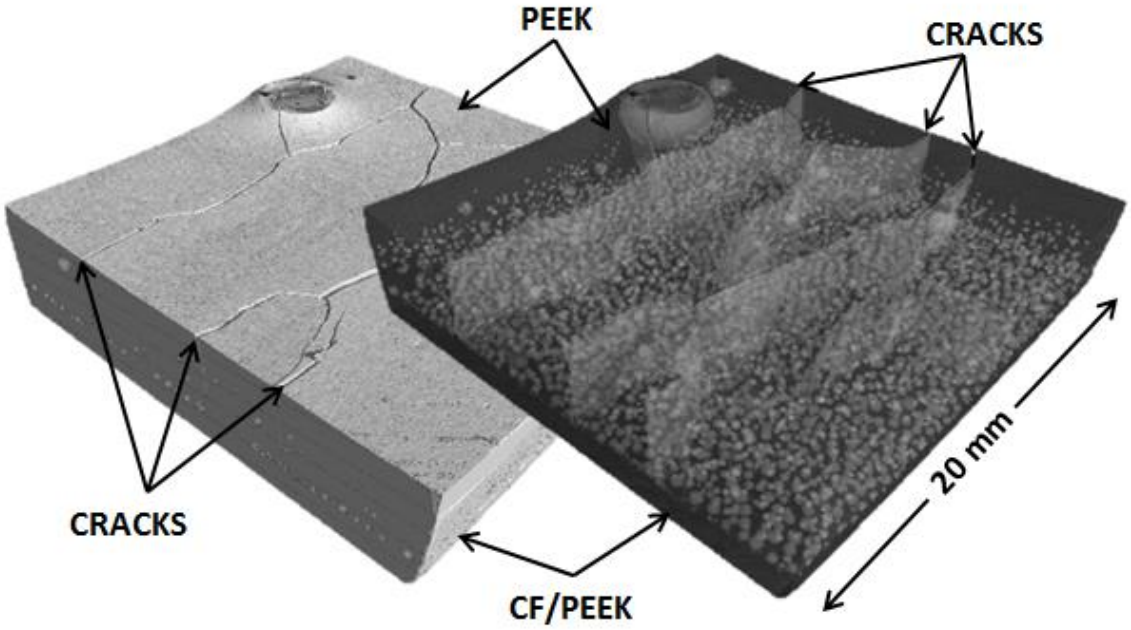

Figure 13. 3-dimensional rendering of a PEEK-CF/PEEK hot plate moulded sample after cryogenic cycling with cracking visible in a solid and transparent view.

A number of conclusions can be drawn from a comparison between the two sets of images. Firstly, and most importantly, the autoclaved CF/PEEK laminates in Fig. 14 are of a significantly superior quality to that of the LATP samples pictured in Fig. 15. The autoclaved samples had no visible regions of debonding, internal defects, or voids between samples. The lack of unbonded regions and gaps in the autoclaved laminates significantly increases their consistency, in regards to material properties, and gives them a consistently lower permeability than their LATP counterparts. Compare this to the LATP sample in Fig. 15 and significant gaps can be seen between individual tape layers in bond regions (7) and (5) which are denoted by the large dark regions in the X-ray images. This is due to the inconsistent width in the CF/PEEK tape used here which restricts the accuracy by which the tape layer can be applied creating an inhomogeneous structure within the laminate.

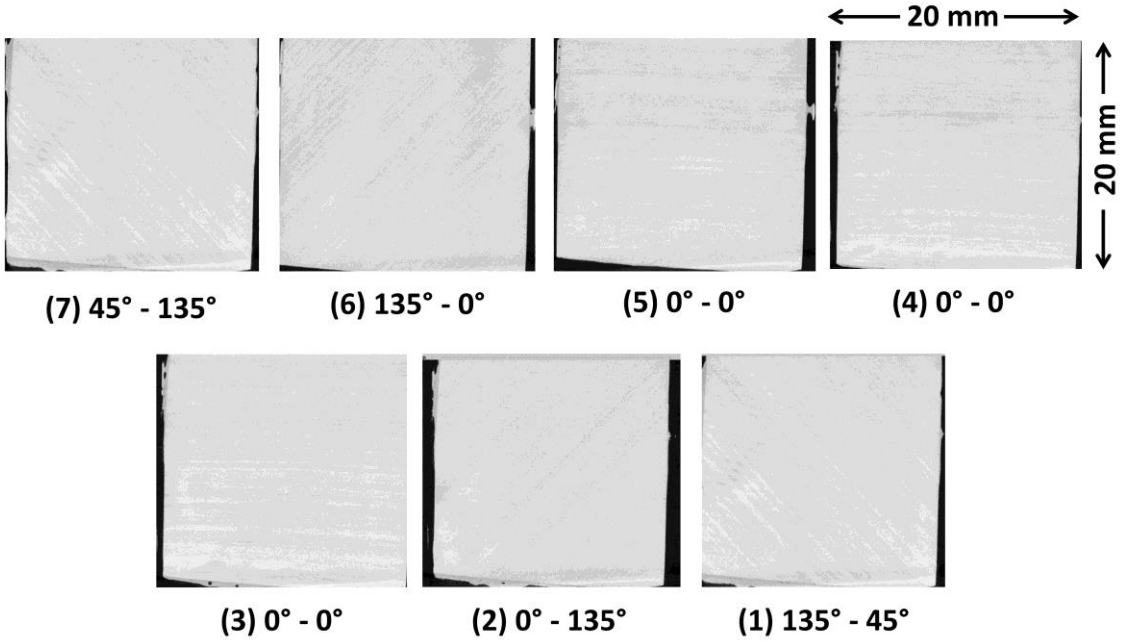

Figure 14. Plan view X-ray CT images of the bond regions between individual layers in a [45°/135°/0°$_4$/135°/45°] Suprem IM7 CF/PEEK autoclaved sample.

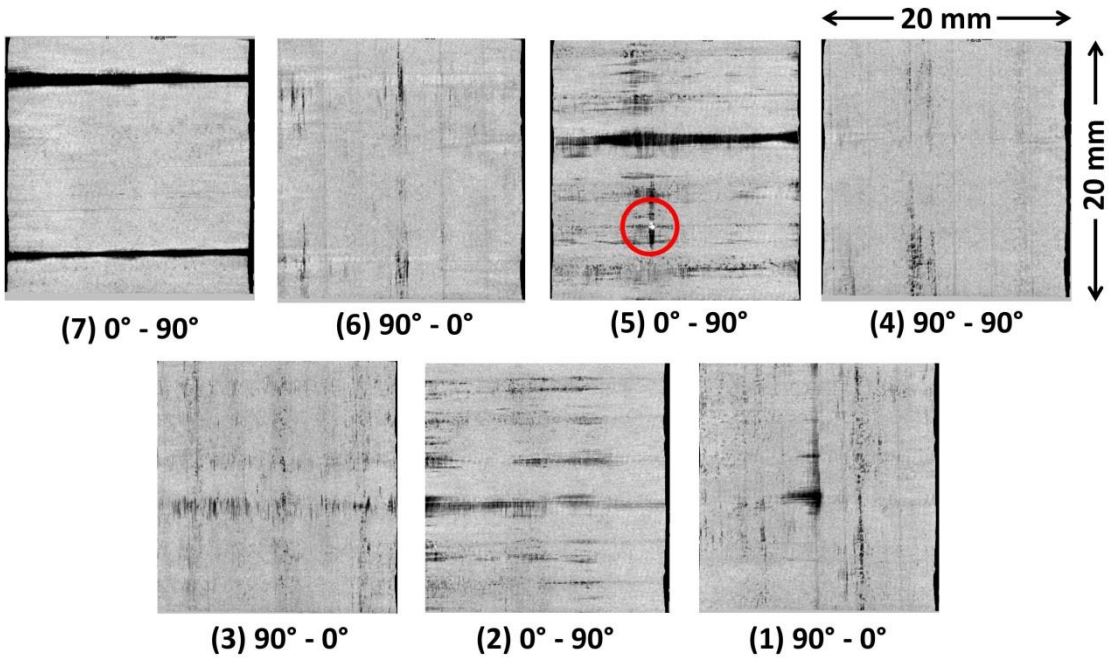

Figure 15. Plan view X-ray images of the bond regions between individual layers in a [0°/90°/0°/90°]$_S$ Suprem IM7 CF/PEEK laminate formed using the LATP process.

The thin, darker regions in bond layers (1) - (4) (the thin black lines contained within these specific X-ray images) are also indicative of unbonded regions which are not fully consolidated. A small fragment of foreign matter has also been included in layer (5) (highlighted by the red circle) which has caused an air gap in the sample. These issues affect the part quality while also affecting permeability [72], since the inclusion of cracks and air voids will increase the rate of permeation through the laminate. A three dimensional view of the voids and defects in the LATP sample has also been provided in Fig. 16, which has highlighted the internal void area within the laminate, again showcasing the relative inconsistencies of the LATP forming process. While the volume of the majority of these voids is quite low, they are thin and long which leads to significantly increased permeability rates throughout these regions which cover large sections of the laminate.

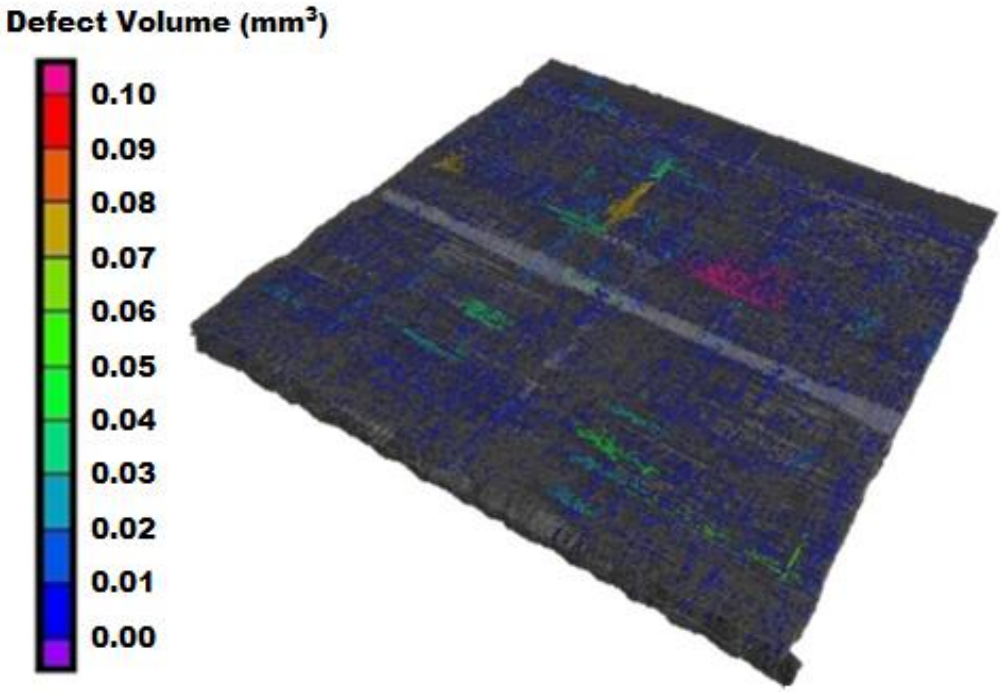

Figure 16. Three dimensional rendering of the internal structure of a $[0°/90°/0°/90°]_S$ Suprem IM7 CF/PEEK LATP sample with internal voids and defects highlighted.

X-ray CT scanning was then used to assess the polymer lined LATP samples, specifically in the area of delamination and crack growth monitoring after repeated cryogenic cycling. Three hot plate moulded PEEK liner samples were over tape-laid with $[0°/90°/0°/90°]_S$ Suprem IM7 CF/PEEK using the LATP process to form a comparative final liner design to the previously hot plate moulded samples. The samples were cycled 50 times with intermittent X-ray scans taken after 1, 2, 3, 5, 10 and 50 cycles. A first analysis of the bond region between the polymer liner and LATP over tape-laid material shows that the consolidation of the overwrap was not perfect, as is evidenced by the large dark regions, in Fig. 17, signifying debonding in the samples before any cycling trials had been performed. This is to be expected as the analysis of LATP CF/PEEK performed earlier showed similar improper consolidation in the CF/PEEK laminates. However, as shown in Fig. 17, the CF/PEEK LATP tape remained bonded to the PEEK liner, even after 50 cycles, with little to no visible change in the bonded regions (the white areas in the X-ray image consisting of a consolidated bond structure). This shows that the bonded regions have a good resistance to debonding under cryogenic cycling.

A cross-like pattern of bonding persists in each image at the liner-overwrap interface. This indicates that the application of the second layer of CF/PEEK tape on the PEEK surface has re-melted the liner surface beneath the first layer and caused consolidation of the liner to the tape-laid material along these regions. This is evidenced by the width between parallel lines being between 12 and 14 mm, i.e. the width of an individual CF/PEEK tape. While the adherence of the overwrap to the liner without delamination over repeated cryogenic cycles is important, the liner's ability to resist cracking over repeated cryogenic cycling is the predominant factor affecting the vessels ability to store cryogenic fuels. Fig. 18 shows that

for two of the three samples tested, the liner material did not contain any cracks after 1, 2, 3, 5, and 10 cryogenic cycles. However, after a further 40 cycles, through thickness cracking was observed in the liner, as shown in Fig. 19, and hence the liner integrity was compromised in between ten and fifty cryogenic cycles. The crack paths appear to originate from the liner-overwrap bond region with the voids on the liner side of the bond line acting as crack initiation points, Fig. 19. The third sample cracked after 1 cycle. This allowed for crack growth to be observed over further cycles to determine the rate of crack growth through the laminate. The cracks had an initial length of 1.0 mm or less. These cracks grew to an average size of 1.6 mm in length over the 10 cycles. This is about half the liner thickness and significantly increases the permeability, due to the reduced effective thickness of the liner. Further cycling to 50 cryogenic cycles caused crack growth through the entire liner thickness and failure of the liner material as a permeation barrier.

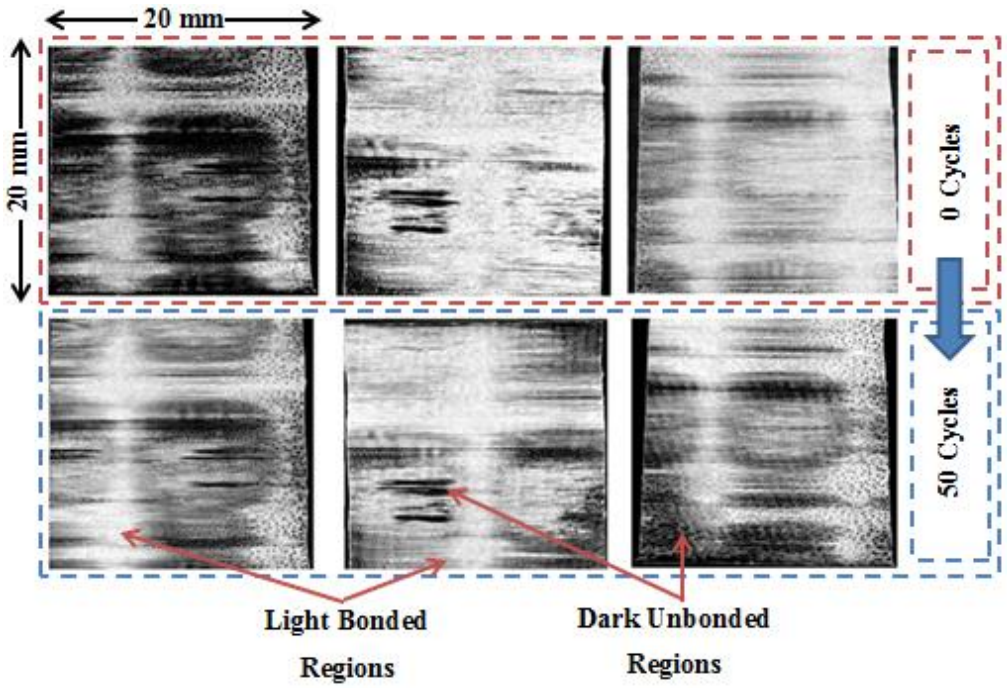

Figure 17. X-ray CT images of the LATP bond region between the CF/PEEK tape and the PEEK liner before and after cryogenic cycling for up to 50 cycles in 3 different samples.

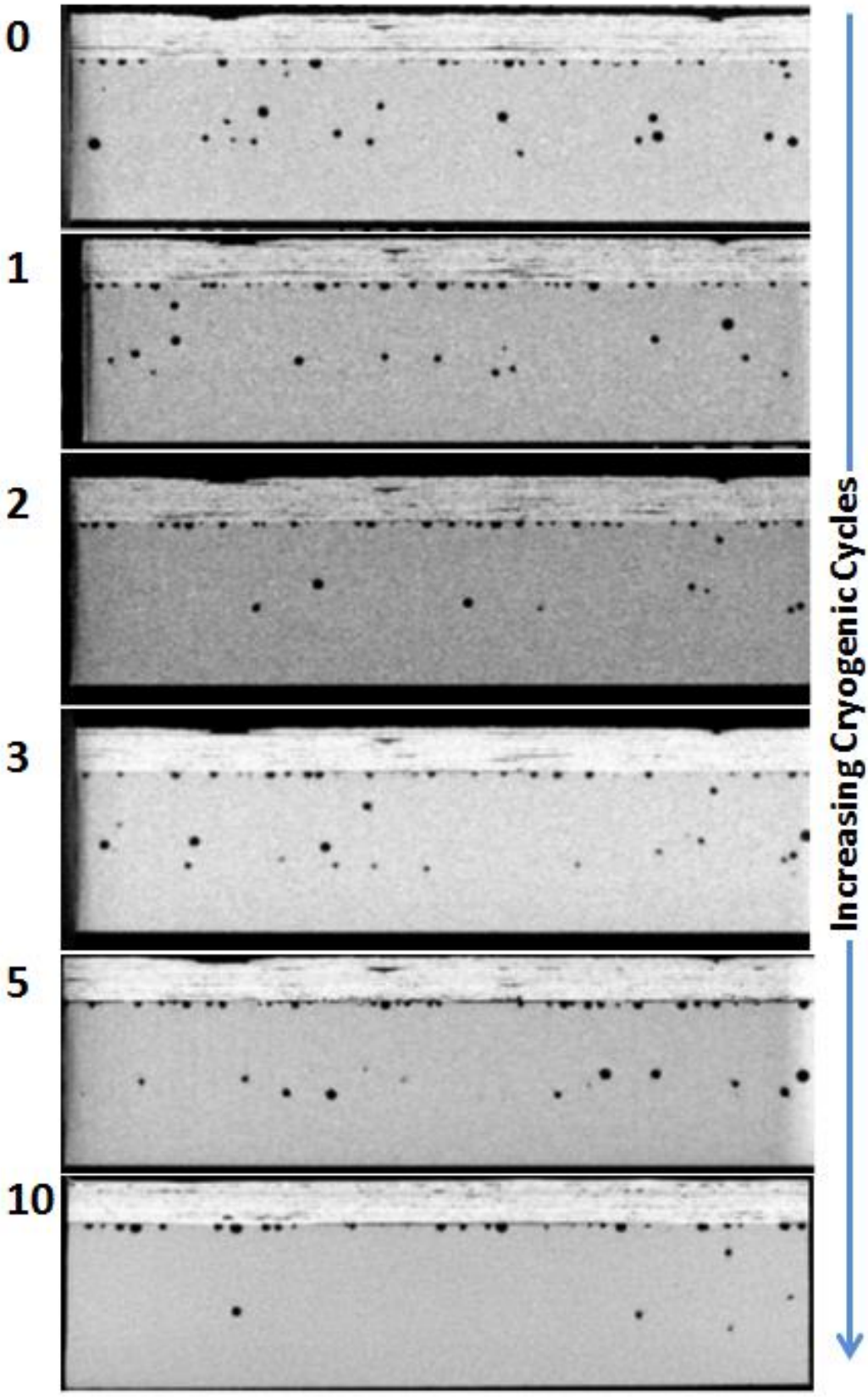

Figure 18. Cross sectional images of a cryogenically cycled $[0°/90°/0°/90°]_S$ CF/PEEK-PEEK LATP laminate after 0, 1, 2, 3, 5, and 10 cycles with no visible cracks present.

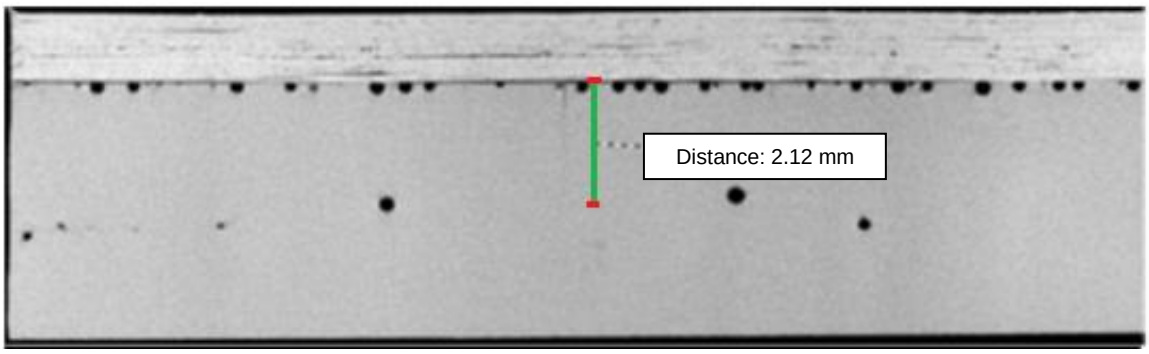

Figure 19. Cross sectional images of a cryogenically cycled $[0°/90°/0°/90°]_S$ CF/PEEK-PEEK LATP laminate after 50 cycles with cracks present.

Nano-Indentation

While the crack resistance for the LATP samples has shown a marked improvement over the hot plate moulded samples, the effects of the laser heating and melting process on the liner surface were also quantified. Fig. 20 shows the modulus results of the individual tests (a minimum of five results were obtained for each data point) showing the change in modulus of the PEEK liner material at the liner-overwrap interface. The PEEK liner material has a significantly lower modulus (at a mean value of 3.5 GPa) near the bond line interface which indicates that the laser heating has altered the material structure and reduced the modulus in this region to a depth of approximately 100 µm, where values settle to around 5 GPa.

This suggests the presence of a laser-affected zone in the PEEK liner material, characterised by a more amorphous region with lower modulus at the bond line interface to a depth of 100 µm, which can be attributed to the rapid heating and cooling effect of the laser on the PEEK substrate. The remainder of the polymer liner below the 100 µm threshold is unaffected by the laser and so retains its higher modulus structure, which is consistent with the slower cool down it undergoes during the rotomoulding process.

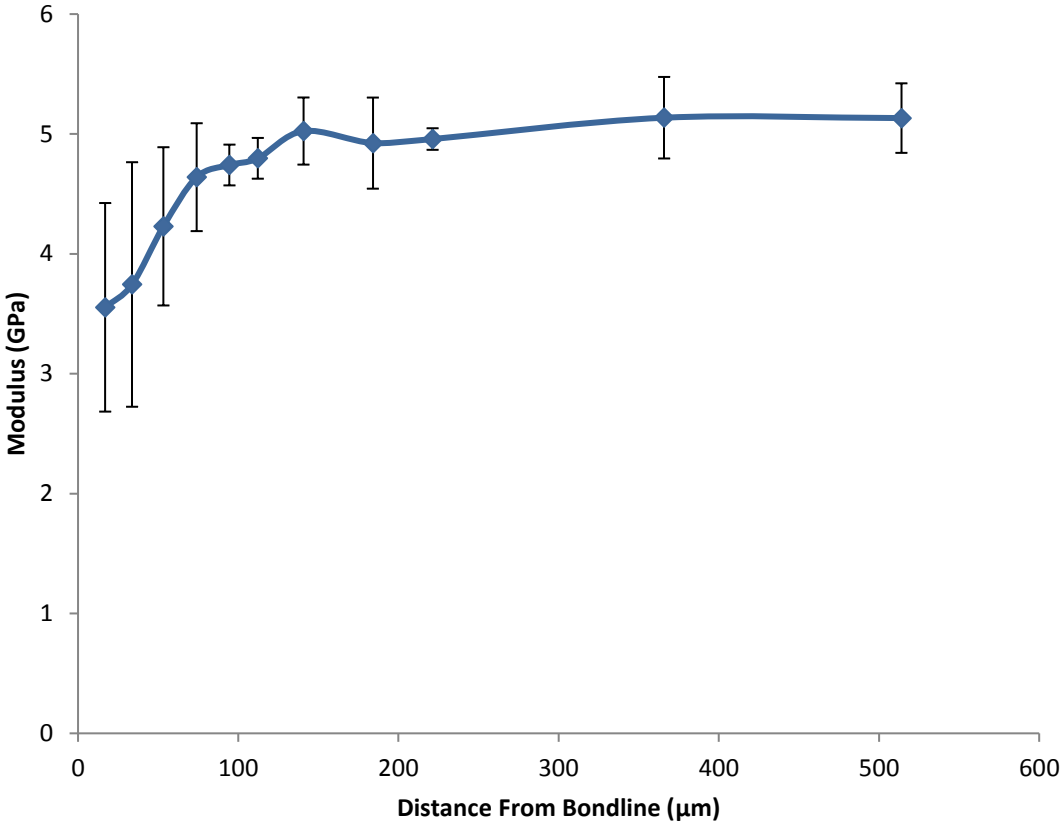

Figure 20. Variation in elastic modulus with distance from the liner-overwrap bond line from nano-indentation testing.

CONCLUSIONS

Reducing the costs of sending payloads to space has been a core aim of the aerospace community over the past number of years. New materials and innovative designs for COPVs have been at the forefront of this research, with significant focus being placed on the development of polymer lined COPVs. A PEEK polymer liner over tape-laid with Suprem IM7 CF/PEEK has been shown to be capable of meeting the low permeability requirements of COPVs. The novel modified rotational moulding process for polymer liner production is a low cost manufacturing method and has the potential to significantly reduce the cost of future COPV liner production. The new moulding process achieved increased wall thickness

consistencies within moulded parts through enhanced thermal control via segregated heating, which was confirmed through thermal imaging and wall thickness measurements. The new rotational moulding system was applied to the rotomoulding of PEEK powder which is reported for the first time, to the authors' knowledge.

Laser assisted tape-placement (LATP) has proven to be an acceptable method for polymer liner over tape-placement with the laying of CF/PEEK tape onto rotomoulded PEEK liners being achieved. Bonding of the CF/PEEK tape to the PEEK liner is not entirely consistent but has remained bonded over extensive cryogenic cycling (up to 50 cycles). LATP laminates of CF/PEEK are not as homogenous as autoclaved samples, with X-ray CT scans and permeability testing showing higher void contents and subsequently higher permeation rates. The majority of microcracking in these laminates occurs during the first cryogenic cycle, as evidenced by the leak rate test results over 10 cryogenic cycles, which is consistent with published research. Some LATP CF/PEEK-PEEK samples cracked after single cryogenic cycles, however smaller samples have resisted crack growth for up to 10 cycles with cracking only occurring after a further 40 cycles.

Nano-indentation testing has shown a reduction in the PEEK liner modulus at the bond line interface to a depth of 100 µm at the liner surface, postulated to be the depth of liner material which is heat-affected by the laser processing. The rapid heating and cooling experienced in this laser-affected zone could be the reason for the lower modulus, due to a lower crystallinity, thus giving an increased toughness and crack resistance to the liner-tape-laid configuration and therefore increasing its crack resistance to levels above those exhibited by hot plate moulded test samples.

ACKNOWLEDGEMENTS

The authors would like to thank the Irish Research Council (IRC) and the European Space Agency (ESA) for joint funding of this research under the Network Partnering Initiative (NPI) and Innovation Triangle Initiative (ITI). They would also like to acknowledge the specific help and technical support provided by Michael Flanagan of NUI Galway, Derrick Doyle and Fintan Doyle of ÉireComposites Teo, and Dr. Terry McGrail and David Jones of the Irish Centre for Composites Research (ICOMP). A final thanks to Prof. Peter McHugh and Dr. Reyhaneh Neghabat Shirazi of NUI Galway for use and training with the nano-indentation testing equipment.

REFERENCES

1. Y. Mizutani, S. Sugimoto, R. Matsuzaki, A. Todoroki, Fundamental Study of Integrity Evaluation Method for COPVs by Means of Acoustic Emission Testing, *J. Acoustic Emission.* 27 (2009) 89-97.
2. H.E. Martinez, J.D. Albright, S.J. D'Amico, J.M. Brewer, J.C. Melcher, Lessons learned from the design, certification, and operation of the space shuttle integrated main propulsion system (IMPS), *47th AIAA/ASME/SAE/ ASEE Joint Propulsion Conference and Exhibit*, California, USA, 2011.
3. J.C. Thesken, P.L.N. Murthy, S.L. Phoenix, N. Greene, J.L. Palko, J. Eldridge, J. Sutter, R. Saulsberry, H. Beeson, A theoretical investigation of composite overwrapped pressure vessel mechanics applied to NASA full scale tests, *NASA/TM-2009-215684*, Ohio Aerospace Institute, Ohio, USA, 2009.

4. J.B. Chang. On Space Flight Pressure Vessel fracture Control, *Fatigue and Fracture Mechanics: 28th Volume, ASTM STP 1321*, ASTM International, Pennsylvania, USA, 1997.
5. M.T. Kezirian, K.L. Johnson, S.L. Phoenix, Composite overwrapped pressure vessels (COPV): Flight rationale for the space shuttle program, *AIAA SPACE 2011 Conference and Exposition*, California, USA, 2011.
6. J.C. Whitehead, C.S. Guernsey, Mars Ascent Propulsion on a Minimum Scale, *Acta Astronaut.* 45 (4-9) (1999) 319-327.
7. M. Duchek, J. Abrams, S. Infeld, S. Jolly, M. Drews, J. Hopkins, Solar electric propulsion orbital debris ferry, vehicle concept and reference mission, *Acta Astronaut.* 116 (2015) 175-185.
8. H. Barthelemy, M. Weber, F. Barbier, Hydrogen storage: Recent improvements and industrial perspectives*, Int. J. Hydrogen. Energ*. 42 (11) (2016) 7254-7262.
9. J. Kast, R. Vijayagopal, J.J. Gangloff Jr., J. Marcinkoski, Clean commercial transportation: Medium and heavy duty fuel cell electric trucks, *Int. J. Hydrogen. Energ.* 42 (7) (2017) 4508-4517.
10. D. Verstraete, P. Hendrick, P. Pilidis, K. Ramsden, Hydrogen fuel tanks for subsonic transport aircraft, *Int. J. Hydrogen. Energ.* 35 (20) (2010) 11085-11098.
11. G. Kawahara, S.F. McCleskey, Titanium Lined, Carbon Composite Overwrapped Pressure Vessel, *32nd AIAA/ASMA/SAE/ASEE Joint Propulsion Conference*, Florida, USA, 1996.
12. W.H. Tam, P.S. Griffin, A.C. Jackson, Design and manufacture of a composite overwrapped pressurant tank assembly, *38th AIAA/ASME/ASME Joint Propulsion Conference*, Indiana, USA, 2002.

13. J.C. Thesken, P.L.N. Murthy, S.L. Phoenix, Composite Overwrap Pressure Vessels: Mechanics and Stress Rupture Lifing Philosophy, *NASA/TM-2009-215683*, Ohio Aerospace Institute, Ohio, USA, 2009.
14. P.L.N. Murthy, Reliability of COPV's Accounting for Margin of Safety on Design Burst, *NASA/TM-2012-217638*, NASA Glenn Research Center, Ohio, USA, 2012.
15. W. Tam, I. Ballinger, D.E. Jaekle, Review and History of ATK Space Systems Commerce - The Past 15 Years, *Internal Report, ATK Space Systems, Commerce,* California, USA, 2008.
16. R. Wei, X. Wang, C. Chen, X. Zhang, X. Xu, S. Du, Effect of surface treatment on the interfacial adhesion performance of aluminum foil/CFRP laminates for cryogenic propellant tanks, *Mater. Des.* 116 (2017) 188-198.
17. A. Hocine, D. Chapelle, L.M. Boubakar, A. Benamar, A. Bezazi, Analysis of intermetallic swelling on the behavior of a hybrid solution for compressed hydrogen storage – Part I: Analytical modeling, *Mater. Des.* 31 (2010) 2435-2443.
18. B.W. Grimsley, R.J. Cano, N.J. Johnson, A.C. Loos, W.M. McMahon, Hybrid composites for LH2 fuel tank structure, *Technical Report 20040086019*, NASA Langley Research Center, Virginia, USA. 2001.
19. G. Remy, F. Benedic, C. Lefloch, The thermoplastic liner: a breakthrough in high pressure vessels technology, *IAASS COPV Safety and Integrity Workshop*, Rome, Italy, 2008.
20. A. Mataloni, F. Betti, M. Biagioni, M. Motta, Elastomeric liner for cryogenic application, *FIAT AVIO-Comprensorio NTEESA 10007 Iss.:2.*, Italy, 2005.

21. S. Claudel, A. Repellin, L. Jageunaud, D. Lacour, A. Bergerot, B. Defoort, Advanced and affordable thermoplastic based composite tank for cryogenic fluid storage, *SAMPE Conference*, Washington State Convention Center, Seattle, USA, 2010.
22. B.R. Murray, S.B. Leen, C.O.A. Semprimoschnig, C.M. Ó Brádaigh, Helium permeability of polymer materials as liners for composite overwrapped pressure vessels, *J. Appl. Polym. Sci*. 133 (29) (2016) 43675-43684.
23. B.R. Murray, S.B. Leen, C.M. Ó Brádaigh, Void distributions and permeability prediction for rotationally moulded polymers, *Proc. Inst. Mech. Eng. L J. Mater. Des. Appl.* 229 (5) (2015) 403-418.
24. L.J. van Rooyen, H. Bissett, M.C. Khoathane, J. Karger-Kocsis, Gas barrier properties of oxyfluorinated graphene filled polytetrafluoroethylene nanocomposites, *Carbon.* 109 (2016) 30-39.
25. R.J. Crawford, M.P. Kearns, *Practical Guide to Rotational Moulding*, Rapra Technology Ltd., Queen's University Belfast, UK, 2003.
26. *Borealis Borecene RM8343 Linear Polyethylene for Rotational Moulding*. http://www.borealisgroup.com/Global/Polyolefins/ - Accessed 26/04/17.
27. *Victrex PEEK 150P Datasheet*. http://www.victrex.com/en/datasheets - Accessed 26/04/17.
28. *Victrex PEEK 150PF Datasheet.* http://www.victrex.com/en/datasheets - Accessed 26/04/17.
29. *Suprem T Datasheet.* https://www.suprem.ch/suprem-t-wide/ - Accessed 26/04/17.
30. *HTSAmptek Heating Tapes.* www.heatingtapes.com/ - Accessed 11/0717.

31. C.M. Stokes-Griffen, P. Compston, T.I. Matuszyk, M.J. Cardew-Hall, Thermal modelling of the laser-assisted thermoplastic tape placement process, *J. Thermoplast. Compos.* 28 (10) (2013) 1445-1462.
32. A.J. Comer, D. Ray, W.O. Obande, D. Jones, J. Lyons, I. Rosca, R.M. O'Higgins, M.A. McCarthy, Mechanical characterisation of carbon fibre-PEEK manufactured by laser-assisted automated-tape-placement and autoclave, *Compos. Part A-Appl. S.* 69 (2015) 10-20.
33. D. Ray, A.J. Comer, J. Lyons, W. Obande, D. Jones, R.M. O'Higgins, M.A. McCarthy, Fracture toughness of carbon fiber/polyether ether ketone composites manufactured by autoclave and laser-assisted automated tape placement, *J. Appl. Polym. Sci*. 132 (11) (2015) 41643-41652.
34. M.A. Khan, P. Mitschang, R. Schledjewski, Identification of some optimal parameters to achieve higher laminate quality through tape placement process, *Adv. Polym. Tech.* 29 (2) (2010) 98-111.
35. Z. Qureshi, T. Swait, R. Scaife, H.M. El-Dessouky, In situ consolidation of thermoplastic prepreg tape using automated tape placement technology: potential and possibilities, *Compos. Part B-Eng.* 66 (2014) 255-267.
36. R. Lichtinger, P. Hörmann, D. Stelzl, R. Hinterhölzl, The effects of heat input on adjacent paths during automated fibre placement, *Compos. Part A-Appl. S*. 68 (2015) 387-397.
37. R. Funck, M. Neitzel, Improved thermoplastic tape winding using laser or direct-flame heating, *Compos. Manuf*. 6 (3-4) (1995) 189-192.
38. C.M. Pistor, S.I. Güçeri, Crystallinity of on-line consolidated thermoplastic composites, *J. Compos. Mater*. 33 (4) (1999) 306-324.

39. W. Grouve, *Weld strength of laser-assisted tape-placed thermoplastic composites*, PhD Thesis, University of Twente, Enschede, the Netherlands, 2012.
40. C.M. Stokes-Griffen, P. Compston, Optical characterisation and modelling for oblique near-infrared laser heating of carbon fibre reinforced thermoplastic composites, *Opt. Laser. Eng.* 72 (2015) 1-11.
41. C.M. Stokes-Griffen, P. Compston, A combined optical-thermal model for near-infrared laser heating of thermoplastic composites in an automated tape placement process, *Compos. Part A-Appl. S*. 75 (2015) 104-115.
42. D.M. Grogan, C.M. Ó Brádaigh, J.P. McGarry, S.B. Leen, Damage and permeability in tape-laid thermoplastic composite cryogenic tanks, *Compos. Part A-Appl. S.* 78 (2015) 390-402.
43. *"ASTM D1434-82. Determining Gas Permeability Characteristics of Plastic Film and Sheeting,"* ASTM International, West Conshohocken, PA, USA, 2009, DOI: 10.1520/D1434-82R09E01.
44. J. Crank, *The Mathematics of Diffusion,* 2nd Edition, Brunel University, Clarendon Press, Oxford, England, 1975.
45. C.W. Extrand, L. Monson, Gas permeation resistance of a perfluoroalkoxy-tetrafluoroethylene compolymer, *J. Appl. Polym. Sci*. 100 (2006) 2122-2125.
46. *DIN EN ISO 11357-1, "Plastics – Differential Scanning Calorimetry (DSC). Part 1: General Principles ,"* DIN Deutsches Institut für Normung e.V., Berlin, Germany, 1997.
47. *"ASTM D3418-12. Transition Temperatures and Enthalpies of Fusion and Crystallisation of Polymers by Differential Scanning Calorimetry,"* ASTM International, West Conshohocken, PA, USA, 2012, DOI: 10.1520/D3418-12E01.

48. R.L. Blaine, *THERMAL APPLICATIONS NOTE – Polymer Heats of Fusion. TN048*, TA Instruments, Denver, USA. http://www.tainstruments.com/main.aspx?n=2&id=181&main_id=367&siteid=11 - Accessed 24/03/15.
49. M. Chen, S.C. Chao, Thermal stability and nonisothermal crystallisation of short fiber reinforced poly(ether ether ketone) composites, *J. Appl. Polym. Sci. Part B*. 36 (1998) 2225-2235.
50. M. Chen, C.T. Chung, Crystallinity of isothermally and nonisothermally crystallised poly(ether ether ketone) composites, *Polym. Composites.* 19 (6) (1998) 689-697.
51. S.L. Gao, J.K. Kim, Cooling rate influences in carbon fibre/PEEK composites. Part 1. Crystallinity and interface adhesion, *Compos. Part A-Appl. S*. 31 (2000) 517-530.
52. J. Brandrup, E.H. Immergut, E.A. Grulke, *Polymer Handbook.* Fourth ed., Wiley-Interscience, 2003.
53. S. Kanehashi, K. Nagai, Analysis of dual-mode model parameters for gas sorption in glassy polymers, *J. Membrane Sci.,* 253 (2005) 117-138.
54. M.N. Fukuya, K. Senoo, M. Kotera, M. Yoshimoto, O. Sakata, Enhanced oxygen barrier property of poly(ethylene oxide) films crystallite-oriented by adding cellulose single nanofibers, *Polymer*. 55 (2014) 5843-5846.
55. E.A. McGonigle, J.J. Liggat, R.A. Pethrick, S.D. Jenkins, J.H. Daly, D. Hayward, Permeability of N2, Ar, He, O2 and CO2 through biaxially oriented polyester films – dependence on free volume, *Polymer.* 42 (2001) 2413-2426.
56. S. Choi, B.V. Sankar, Gas permeability of various graphite/epoxy composite laminates for cryogenic storage system, *Compos. Part B-Eng.* 39 (2008) 782-791.

57. V.T. Bechel, M.B. Fredin, S.L. Donaldson, R.Y. Kim, J.D. Camping, Effect of stacking sequence on micro-cracking in a cryogenically cycled carbon/bismaleimide composite, *Compos. Part A-Appl. S*. 34 (2003) 663-672.

58. V.T. Bechel, R.Y. Kim, Damage trends in cryogenically cycled carbon/polymer composites, *Compos. Sci. Technol*. 64 (2004) 1773-1784.

59. D.M. Grogan, S.B. Leen, C.O.A. Semprimoschnig, C.M. Ó Brádaigh, Damage characterisation of cryogenically cycled carbon fibre/PEEK laminates, *Compos. Part A-Appl. S.* 66 (2014) 237-250.

60. C. Henaff-Gardin, M.C. Lafarie-Frenot, D. Gamby, Doubly periodic matrix cracking in composite laminates Part 2: Thermal biaxial loading, *Compos. Struct*. 36 (1996) 131-140.

61. R.D. Crouch, S.B. Clay, C. Oskay, Experimental and computational investigation of progressive damage accumulation in CFRP composites, *Compos. Part B-Eng*. 48 (2013) 59-67.

62. J. Kastner, B. Plank, A. Reh, D. Salaberger, C. Heinzl, Advanced X-ray tomographic methods for quantitative characterisation of carbon fibre reinforced polymers, *4th International Symposium on NDT in Aerospace 2012*, Augsburg, Germany, November 13-15, 2012.

63. P.J. Schilling, B.R. Karedla, A.K. Tatiparthi, M.A. Verges, P.D. Herrington, X-ray computed microtomography of internal damage in fiber reinforced polymer matrix composites, *Compos. Sci. Technol*. 65 (2005) 2071-2078.

64. S. Roy, M. Benjamin, Modeling of permeation ad damage in graphite/epoxy laminates from cryogenic fuel storage, *Compos. Sci. Technol*. 64 (2004) 2051-2065.

65. A. Nair, S. Roy, Modelling of permeation and damage in graphite/epoxy laminates for cryogenic tanks in the presence of delaminations and stitch cracks, *Compos. Sci. Technol.* 67 (2007) 2592-2605.

66. V.T. Bechel, J.D. Camping, R.Y. Kim, Cryogenic/elevated temperature cycling induced leakage paths in PMCs, *Compos. Part B-Eng*. 36 (2005) 171-182.

67. V.T. Bechel, M. Negilski, J. James, Limiting the permeability of composites for cryogenic applications, *Compos. Sci. Technol*. 66 (2006) 2284-2295.

68. T. Yokozeki, T. Aoki, T. Ogasawara, T. Ishikawa, Effects of layup angle and ply thickness on matrix crack interaction in contiguous plies of composite laminates, *Compos. Part A-Appl. S.* 36 (2005) 1229-1235.

69. T. Yokozeki, T. Ogasawara, T. Ishikawa, Evaluation of gas leakage through composite laminates with multilayer matrix cracks: Cracking angle effects, *Compos. Sci. Technol*. 66 (2006) 2815-2824.

70. D.M. Grogan, S.B. Leen, C.M. Ó Brádaigh, An X-FEM based methodology for fatigue delamination and permeability of composites, *Compos. Struct*. 107 (2014) 205-218.

71. D. Grogan, C.M. Ó Brádaigh, S.B. Leen, A combined XFEM and cohesive zone model for composite laminate microcracking and permeability, *Compos. Struct.* 120 (2015) 246-261.

72. M. Flanagan, D.M. Grogan, J. Goggins, S. Appel, K. Doyle, S.B. Leen, C.M. Ó Brádaigh, Permeability of Carbon Fibre PEEK Composites for Cryogenic Storage Tanks of Future Space Launchers, *Compos. Part A-Appl.* 101 (2017) 173-184.

73. *"ASTM E2546-15. Standard Practice for Instrumented Indentation Testing,"* ASTM International, West Conshohocken, PA, USA, 2015, DOI: 10.1520/E2546-15.

74. R. Neghabat Shirazi, Y. Rochev, P. McHugh, Nanoindentation of solvent-cast and compression-moulded poly(lactic-co-glycolic acid) to determine elastic modulus and hardness, *Polym. Test*. 50 (2016) 111-118.
75. R. Neghabat Shirazi, F. Aldabbagh, A. Erxleben, Y. Rochev, P. McHugh, Nanomechanical properties of poly(lactic-co-glycolic) acid film during degradation, *Acta Biomaterialia.* 10 (2014) 4695-4703.
76. D.J. Shuman, A.L.M. Costa, M.S. Andrade, Calculating the elastic modulus from nanoindentation and microindentation reload curves, *Mater. Charact*. 58 (2007) 380-389.
77. W.C. Oliver, G.M. Pharr, Measurement of hardness and elastic modulus by instrumented indentation: Advances in understanding and refinements to methodology, *J. Mater. Res.* 19 (1) (2004) 3-20.
78. P.J. Rae, E.N. Brown, E.B. Orler, The mechanical properties of poly(ether-ether-ketone) with emphasis on the large compressive strain response, *Polymer*. 48 (2007) 598-615.
79. R.C. Powles, D.R. McKenzie, S.J. Meure, M.V. Swain, N.L. James, Nanoindentation response of PEEK modified by mesh-assisted plasma immersion ion implantation, *Surf. Coat. Tech*. 201 (2007) 7961-7969.
80. T. Iqbal, B.J. Briscoe, P.F. Luckham, Surface plasticization of poly(ether ether ketone), *Eur. Polym. J*. 47 (2011) 2244-2258.
81. W. Kaczorowski, D. Batory, W. Szymanski, P. Niedzielski, Evaluation of the surface properties of PEEK substrate after two-step plasma modification: Etching and deposition of DLC coatings, *Surf. Coat. Tech.* 265 (2015) 92-98.

82. A. Molazemhosseini, H. Tourani, M.R. Naimi-Jamal, A. Khavandi, Nanoindentation and nanoscratching responses of PEEK based hybrid composites reinforced with short carbon fibers and nano-silica, *Polym. Test.* 32 (2013) 525-534.

83. J.R. Gregory, S.M. Spearing, Nanoindentation of neat and in situ polymers in polymer-matrix composites, *Compos. Sci. Tech.* 65 (2005) 595-607.

84. M. Sattari, A. Molazemhosseini, M.R. Naimi-Jamal, A. Khavandi, Nonisothermal crystallization behaviour and mechanical properties of PEEK/SCF/nano-SiO2 composites, *Mater. Chem. Phys.* 147 (2014) 942-953.

85. Y. Zhao, T.C. Ovaert, Error estimation of nanoindentation mechanical properties near a dissimilar interface via finite element analysis and analytical solution methods, *J. Mater. Res.* 25 (12) (2010) 2308-2316.

86. A.E. Fick, Ueber Diffusion, *Ann. Phys-Leipzig*. 170 (1) (1855) 59–86.

87. S.A. Sabzevari, M. Sadeghi, A. Mehrabani-Zeinbad, A multi-structural model for prediction of effective gas permeability in mixed-matrix membranes, *Macromol. Chem. Physic.* 214 (2013) 2367-2376.

88. B.R. Murray, *Characterisation of rotationally moulded polymer liners for low permeability cryogenic applications in composite overwrapped pressure vessels*, PhD Thesis, National University of Ireland Galway, Galway, Ireland, 2016.